February 2000

Final Report

to

US AIR FORCE OFFICE OF SCIENTIFIC RESEARCH/NA
801 N Randolph St., Rm. 732
Arlington VA 22203-1977 USA

ATTN: DR. JULIAN M. TISHKOFF
<julian.tishkoff@afosr.af.mil>

TRANSPORT AND INTERFACIAL PHENOMENA IN MULTI-PHASE COMBUSTION SYSTEMS

AFOSR Grant No. 97-1-0266
Principal Investigator: Daniel E. Rosner
Yale University, Department of Chemical Engineering
High Temperature Chemical Reaction Engineering Laboratory
New Haven, CT 06520-8286, USA

Period Covered: April 1, 1997- November 30, 1999

TRANSPORT AND INTERFACIAL PHENOMENA IN MULTIPHASE COMBUSTION SYSTEMS

AFOSR Grant No. 97-1-0266
Principal Investigator: **Daniel E. Rosner**
Yale University, Department of Chemical Engineering
High Temperature Chemical Reaction Engineering Laboratory
New Haven, CT 06520-8286, USA

TABLE OF CONTENTS

1. INTRODUCTION 1

2. PRINCIPAL RESEARCH ACCOMPLISHMENTS

2.1 Laser-Induced Incandescence (LII) for Soot Measurements: New 'Modalities' 1

2. 2. Development of 'Thermophoresis-Based' Particle Diagnostic Techniques 1

2. 3 Simulation Methods for Aerosol Populations Described by Two (or More) "State Variables" 2

2.4 Prediction of Particle Deposition from Soot Populations 2

3. ADMINISTRATIVE INFORMATION: PRINCIPAL PERSONNEL, PRESENTATIONS, APPLICATIONS, "TECHNOLOGY TRANSFER"

3.1 Principal Research Personnel 3

3.2 Cooperation with US Industry 3

3.3 Comments on Presentations, Research Training, and Pedagogical Impact 4

3.4 Applications of Yale-OSR-Derived Research Results 4

4. CONCLUSIONS 4

5. REFERENCES

5.1 BACKGROUND REFERENCES CITED 5

5.2 PUBLICATIONS (APPEARED) BASED ON GRANT AFOSR 97-1-0266 7

5.3 AFOSR 97-1-0266 WORK IN PRESS, OR SUBMITTED FOR PUBLICATION 8

6. APPENDIX 1 (Form 298 for Previously Unreported AFOSR 97-1-0266 *Published* Papers) 8
PIADC INFORMATION

REPORT DOCUMENTATION PAGE

AFRL-SR-BL-TR-00-

0204

1. AGENCY USE ONLY (Leave blank)	2. REPORT DATE	3. REPORT TYPE AND DATES COVERED
	February 2000	FINAL REPORT April 1,'97-Nov 30,'99

4. TITLE AND SUBTITLE

(U) **TRANSPORT AND INTERFACIAL PHENOMENA IN MULTIPHASE COMBUSTION SYSTEMS**

5. FUNDING NUMBERS

PE - 61102F
PR - 2308
SA - BS
G-F49620-97-1-0266

6. AUTHOR(S)

Daniel E. Rosner (PI)

7. PERFORMING ORGANIZATION NAME(S) AND ADDRESS(ES)

Yale University
High Temperature Chemical Reaction Engineering Laboratory
Department of Chemical Engineering
PO Box 208286 YS, New Haven, CT 06520-8286 USA

8. PERFORMING ORGANIZATION REPORT NUMBER

9. SPONSORING/MONITORING AGENCY NAME(S) AND ADDRESS(ES)

AFOSR/NA
801 N Randolph St., Rm. 732
Arlington VA 22203-1977

10. SPONSORING/MONITORING AGENCY REPORT NUMBER

11. SUPPLEMENTARY NOTES

See, also, Annual Reports dated Sept.'97, Sept.'98, Sept. '99.

12a. DISTRIBUTION/AVAILABILITY STATEMENT

Approved for public release; distribution is unlimited

12b. DISTRIBUTION CODE

13. ABSTRACT (*Maximum 200 words*)

Results of a 3-year research program, leading to 17 archival papers, are summarized here, covering the four basic areas: A) Laser-Induced Incandescence (LII) for soot measurements at atmospheric pressure and high pressures; B) 'Thermophoresis-based' particle diagnostic techniques; C) Simulation methods for aerosol populations described by two (or more) "state variables"; and D) Particle deposition from soot populations. As examples, we found that the small Knudsen number (*eg.* high pressure) limit, Laser-Induced Incandescence (LII) *can* be used to infer *aggregate* size distributions, pdf(N). This requires improved estimates of the optical and heat transfer properties of fractal aggregates, also obtained under the present program (Filippov and Rosner, 1998,1999, Filippov *et al.*1999). Our thermophoresis/soot *deposition* research has led to a novel and quite convenient method (called 'TPD') to track local *soot volume fractions* in laminar flames, most recently including flames deliberately 'doped' with possible soot pre-cursors. A versatile Monte-Carlo-based (MC-) simulation of the *population balance equation* PBE has also been developed (Tandon and Rosner,1999, Rosner and Yu, 1999) and successfully demonstrated for the important 2-state variable case in which each non-spherical particle in the population is characterized by its *volume* v and *surface area*, a. Even in this *bi-variate* case, "self-preserving" (constant *shape* pdf) asymptotic solutions have been found (Tandon and Rosner,1999; in both the *continuum* and *free-molecular* limits (Rosner and Yu,1999), and their physically important 'mixed moments' calculated.

14. SUBJECT TERMS

Laser-induced incandescence. soot morphology , aggregated particles, particle mass transport thermophoresis, Brownian diffusion, particle sampling, nano-particle formation/restructuring in flames, deposition rate theory

15. NUMBER OF PAGES

3+30=33

16. PRICE CODE

17. SECURITY CLASSIFICATION OF REPORT	18. SECURITY CLASSIFICATION OF THIS PAGE	19. SECURITY CLASSIFICATION OF ABSTRACT	20. LIMITATION OF ABSTRACT
Unclassified	Unclassified	Unclassified	UL

1. INTRODUCTION

The performance of aircraft gas turbine engines under sooting conditions and/or ramjets burning slurry fuels (leading to oxide aerosols and deposits), depends upon the formation and transport of small particles of complex morphology, often in highly non-isothermal combustion gas boundary layers (BLs). Aggregate formation / transport are also important in chemical reactors used to synthesize/process aerospace materials, including turbine blade coatings, optical waveguides, ceramic precursor powders,...). Accordingly, this research was directed toward providing chemical propulsion system engineers with rational new predictive techniques to deal with *particle formation-transport-deposition phenomena*, accounting for significant non-spherical particle morphology effects. An interactive experimental/theoretical approach was used to gain an understanding of performance-limiting mass/energy transfer-phenomena at or near interfaces. This included the development/exploitation of laboratory burners and new diagnostic/characterization techniques (Sections 2.1,2.2). Resulting experimental data, together with the predictions of asymptotic theories were then used to propose and verify rational engineering correlations for future design/optimization.

2. SUMMARY OF PRINCIPAL RESEARCH ACCOMPLISHMENTS‡

Most of the results obtained under Grant AFOSR 97-1-0266 can be divided into the subsections below:

2.1 Laser-Induced Incandescence (LII) for Soot Measurements: New 'Modalities'

While instantaneous, local soot volume fractions and spherule sizes are sufficient for some purposes (especially in predicting the structure of atmospheric pressure flames), a knowledge of the *aggregate* size distribution (ASD or *pdf(N)* , where N is the number of spherules in a 'fractal-like' aggregate) is essential to predict the radiative properties and, say, health effects of sooting combustors. Rapid response LII access to such information would also permit the development of local aggregate number density pdfs and relevant 'scatter' diagrams in turbulent sooting flows, thereby facilitating the development of more realistic soot models for such environments. Under the present grant we carried out an analysis (Filippov *et al.* 1999a); which demonstrated, for the first time, that in the small Knudsen number (*eg.* high pressure) limit, LII *can* be used to infer *aggregate* size distributions. We exploited an improved theoretical knowledge of the optical and heat transfer properties of fractal aggregates (Filippov and Rosner, 1998,1999, Filippov *et al.*1999b). We showed that the 'accessible' domain (on the plane of aggregate population *spread* vs. geometric mean number of spherules per aggregate, N_g) includes most soot cases of practical interest.

2. 2. Development of 'Thermo-Phoresis-Based' Particle Diagnostic Techniques

In this program we developed/demonstrated two thermophoresis-based methods for measuring absolute local *soot volume fractions*, f_p, in both co-flow and counterflow laminar diffusion flames). The first, called *Thermocouple Particle Densitometry* (TPD)(McEnally *et.al.*(1997)), exploits the laws governing thermocouple response to *thermophoretic soot deposition*, as first suggested by the PI in 1985. This 'TPD' research has led to a novel and quite convenient method to track local soot volume fractions in laminar flames, most recently including flames deliberately 'doped' with possible soot pre-cursors (McEnally and Pfefferle,1998). Remarkably, the method responds to transparent soot (condensed PAHs, important in soot inception) to which ordinary laser light extinction (LLE) is "blind" (McEnally *et al.*, 1998, Koylu *et al.* 1998). A combination of TPD and more classical methods of analysis is expected to shed new light on the role these ubiquitous "transparent" particles, found very early in hydrocarbon vapor/air diffusion flames, play in the overall soot formation process.

‡ For research collaborators consult Sections 3, 5

The second, related technique, which we call *Thermophoretic Sampling Particle Diagnostic* (TSPD) (Koylu, *et.al.* (1997)) is an extension of TEM-based thermophoretic sampling to also obtain absolute, local soot volume fractions, again making use of the laws governing *thermophoretic soot deposition* (*eg.*, Rosner *et..al.* (1991,1992)).

2.3 Simulation Methods for Aerosol Populations Described by 2 (or More)"State Variables"

Based on the expectation that 'sectional' (finite-difference) methods will become problematic for the ultimate prediction of *multi-variate pdfs* for sooting, turbulent combustors, we have developed/illustrated a more versatile Monte-Carlo-based (MC-) simulation of the *population balance equation* PBE (Tandon and Rosner,1999, Rosner and Yu, 1999) and successfully demonstrated the efficacy of this approach for the an important 2-state variable case in which each non-spherical particle in the population is characterized by its *volume* v and *surface area* , a. Even in this *bivariate* case we have found "self-preserving" (constant *shape* pdf) asymptotic solutions (Tandon and Rosner,1999(continuum regime); and, for the free-molecule regime, Rosner and Yu,1999). While these "self-preserving" solutions may not apply apply locally to the dynamical situation of many real flames, including the TMA-seeded atmospheric pressure counter-flow diffusion flames on which we have considerable experimental data (Xing *et.al.*,1997,1999), they are of considerable theoretical interest, and can be used to predict many observable properties of 'coagulation-aged' aerosol populations, including *mass deposition rates* (Rosner *et.al.*(1998,2000)). As a corollary of this research, we have developed methods to predict the decisive mean spherule size (which fixes the specific surface area of such aerosols)(see, Xing and Rosner,1999), and even the spherule size distribution (Rosner and Yu(2000)).

2.4 Prediction of Particle <u>Deposition</u> from Soot Populations

The fact that smokes or mists of aerospace and environmental interest are comprised of particles both large and small compared to the prevailing gas mean-free-path inevitably complicates accurate predictions of, say, *total mass deposition rates* to confining walls by the mechanism of convective-Brownian diffusion (Sc>>1), or thermophoresis, across laminar or turbulent boundary layers. However, since all individual particle transport properties are sensitive to the prevailing Knudsen number based on particle diameter, this must be accurately taken into account. In the present program we extended previous results from this laboratory to show how deposition rates from a flowing stream of coagulation-aged polydispered spherical particles in the Knudsen *transition* regime can be predicted by systematically correcting results more easily calculated for the (hypothetical) reference case of mono-dispersed spheres, either in the *continuum* or free-molecule limit. For this purpose we carried out "once-and-for-all" quadratures over the Cunningham-Millikan "slip-flow" function, and the Talbot thermophoretic function (Rosner and Khalil,2000) with appropriate quasi-self-preserving particle size distribution (PSD-) functions, using recent information on the effective spreads ($\sigma_{g,eff}$) of these near-log-normal PSDs associated with Brownian coagulation in the transition regime. Whether the deposition mechanism is Brownian diffusion (Rosner,1998) or thermophoresis (Rosner and Khalil(2000)), this led to rational "universal" correlations, in terms of the prevailing Knudsen number based on *mean* particle size in the population, which will drastically simplify and accelerate such particle deposition rate calculations in the future.

3. ADMINISTRATIVE INFORMATION: PRINCIPAL PERSONNEL, PRESENTATIONS, APPLICATIONS, "TECHNOLOGY TRANSFER"

The following sub-sections summarize some pertinent facets of the abovementioned Yale HTCRE Lab/AFOSR (nominally 3 year-) research program of *management* interest:

3.1 Principal Research Personnel

The present results (summarized in Sections 2 and 5 and the 17 papers prepared under this program) are mainly due to the contributions of the individuals listed in Table 3.1-1, which also indicates the overall role of each researcher. It is noteworthy that, in addition to the results themselves, this program has simultaneously contributed to the research training of PhD students: M. Zurita, and Y. Xing. The latter, recently completed a post-doctoral position at Johns Hopkins Univ., and was runner-up for the 1999 ACS/Colloid Div.*V. LaMer Award* (based on outstanding dissertation research). He is now in an excellent position to make future contributions to technologies oriented toward high-tech aerospace materials synthesis/processing.

Table 3.1-1 Summary of *Principal Research Participants*[a] on AFOSR Grant: 97-1-0266 :
TRANSPORT PHENOMENA AND INTERFACIAL PHENOMENA IN MULTIPHASE COMBUSTION SYSTEMS

Name	Status[a]	Date(s)	Principal Research Activity[b]
Filippov, A.V.	PDRA-RS/S	9/97-11/99	LII theory for *pdf(d$_1$)* and *pdf(N)*
Rosner, D.E.	PI	4/97 -11/99	Program direction-dep. theory/exp
Xing, Y.	GRA-PDRA	4/97 -6/98	Particle prod./char. In CDFs
Yu, S.	PDRA	10/98-7/99	MC Simulation of soot coagulation
Zurita,M	GRA	1/99-11/99	LII theory; Aggregate properties

[a] PDRA=Post-doctoral Research Asst GRA= Graduate Research Assistant (V=Visiting)
PI = Principal Investigator [b] See Sections 5.2,5.3 for specific references cited in text (Section 2)
RS/S=Reseach Scientist/Scholar

3.2 Cooperation with US Industry

While the research summarized here was principally supported by AFOSR under Grant 97-1-0266, the Yale HTCRE Laboratory has also been the beneficiary of occasional smaller grants from U.S. industrial corporations, including groups within ALCOA, GE, DuPont, Union Carbide (now Advanced Ceramics Corp.) and Shell, as well as the feedback and advice of scientists/engineers from these/other corporations. We appreciate this level of collaboration, and expect that it will accelerate inevitable applications of our results in areas relevant to their technological objectives (see, also, Section 3.4, below).

Periodically, our results are picked up and used by aerospace-oriented industrial contractors, or corporations engaged in ancillary chemical industry. However, no *bona-fide* "Technical Transition" was identified by the PI during this particular interval.

3.3 External Presentations, Research Training, and Pedagogical Impact

Apart from the 17 publications cited above and itemized in Sections 5, we have presented some 20 technical talks on the subject matter of this Grant. With few exceptions these have been at national meetings of the Combustion Inst., AIChE, and AAAR, or as University seminars (as documented in our earlier Annual Reports on this grant).

The pedagogical impact of the PI's AFOSR research will be considerably augmented when Dover Publications (Mineola, NY) markets an updated paperback reprint of his 1986 textbook-treatise during the summer of 2000. This 'reprint' will actually contain a 50 page Supplement which cites many recent papers, including those supported by this Grant.

3.4 *Applications* of Yale-HTCRE Lab Research Results; Technology Transfer

As an indication of the worldwide scientific impact* of this 3-year OSR-supported program, some 150 citations have appeared under the PI's name: Rosner, D.E. in *Science Citation Index*. It has been gratifying to see direct applications of this generic AFOSR-supported particle and vapor mass transfer research in more applications-oriented investigations reported in recent years, as documented in our earlier Annual Reports. During this reporting period there were apparently no new *bona-fide* 'transitions' to report, although our recent OSR research on particle *deposition* and impact-induced *erosion* is being used in the land-based combustion turbine industry, including that concerned with energy recovery at chemical plants (Private Communications related to the PI's consulting activities). Applications in other fundamentally-oriented research programs are easier to discover and track. For example, the PI has become aware that 'TPD', a thermophoretically-based technique for determining local soot volume fractions and temperatures in laminar flames (see Section 2.2), is currently being used at UCLA, VPI and UTRC. This technique, a 'byproduct' of our OSR-sponsored particle *deposition* research (Section 2.4), is quite attractive because it is simple, completely independent of particle *optical* properties, and applicable to *very* low soot volume fractions.

4. CONCLUSIONS

This 3-year AFOSR program was motivated by the fact that the ability to reliably predict the local concentration, sizes, transport properties and stability of *aggregated* flame-generated *particles* (carbonaceous soot, B_2O_3, Al_2O_3, ...), often in the size range of only tens of nanometers, in high pressure, high temperature environments, is important for many technologies relevant to the U.S.A.F., especially jet engine combustor design. As one important overall result, we have shown that soot aggregates from a wide variety of organic and inorganic combustion systems exhibit mechanistically significant *morphological* and transport property similarities (Rosner et.al.,1997, Koylu *et.al.*,1995,1997, Xing *et.al.*, 1997,1999). Indeed, our results for the *transport properties of soot aggregates* can now be used in more accurate models of soot dynamics in l*aminar and turbulent* flames. Moreover, we have also provided properties needed to correctly interpret the results of recently introduced laser diagnostics as applied in research on soot formation/suppression at high pressures (*eg.*, laser-induced incandescence (LII)). These experimental techniques, together with closely coupled theoretical calculations of particle birth/dynamics in counterflow diffusion flames and mixing/boundary layers, have led to a significantly improved understanding of combustion-generated ultra-fine particles, including their sampling, coagulation, restructuring and deposition dynamics.

5. REFERENCES

5.1 BACKGROUND PUBLICATIONS

Eisner, A.D. and Rosner, D.E., "Experimental Studies of Soot Particle Thermophoresis in Non-Isothermal Combustion Gases Using Thermocouple Response Techniques", *Combustion and Flame* **61**, 153-166(1985); see, also: *J PhysicoChemical Hydrodynamics* (Pergamon) **7** , 91-100 (1986)

Farias, T.L., Koylu, U.O., and Carvalho, M.G., "Effects of Polydispersity of Aggregates and Primary Particles on Radiative Properties of Simulated Soot", *J. Quant. Spectros. Radiat. Transfer* **55** (3) 357-371 (1996)

Fernandez de la Mora, J. and Rosner, D.E., "Inertial Deposition of Particles Revisited and Extended: Eulerian Approach to a Traditionally Lagrangian Problem", PCH *Physicochemical Hydrodynamics* (Pergamon) **2** (1), 1-21, (1981)

Filippov, A.V., Rosner, D.E, Xing, Y., Long, M. and Schaffer, A.(1998), "Comparison Between Detailed LII Method and TEM Analysis for Ultrafine Soot Particles in Flames", *27th Combustion Symposium*, Boulder CO; Poster W5G05

Garcia-Ybarra, P. and Castillo, J.L., "Mass Transfer Dominated by Thermal Diffusion in Laminar Boundary Layers", *J. Fluid Mechs.*, **336**, 379-409 (1997)

Gomez, A., and Rosner, D.E., "Thermophoretic Effects on Particles in Counterflow Laminar Diffusion Flames " *Comb Sci &Tech* **89**, 335-362 (1993)

Khalil, Y. F. and Rosner, D.E., "Erosion Rate Prediction and Correlation Technique for Ceramic Surfaces Exposed to High-Speed Flows of Abrasive Suspensions", *WEAR* **201**, 64-79 (1996)

Konstandopoulos, A.G., Labowsky, M J., and Rosner, D.E., "Inertial Deposition of Particles From Potential Flows Past Cylinder Arrays", *J. Aerosol Sci* (Pergamon) **24** (4) 471-483 (1993)

Konstandopoulos, A.G. and Rosner, D.E.,"Inertial Effects on Thermophoretic Transport of Small Particles to Walls With Streamwise Curvature---I. Theory, *Int. J. Heat Mass Transfer* (Pergamon) **38** (12) 2305-2315 (1995)

Konstandopoulos, A.G. and Rosner, D.E.,"Inertial Effects on Thermophoretic Transport of Small Particles to Walls With Streamwise Curvature---II. Experiment, *Int. J. Heat Mass Transfer* (Pergamon)**38** (12) 2317-2327 (1995)

Konstandopoulos, A.G., Kostoglou, M., and Rosner, D. E., "Shape Evolution of Particulate Deposits Growing on Cylinders in Cross-flow", *Proc. 3d International Particle Technology Congress,* Paper # 284, Inst. ChE(UK), July 1998

Koylu, U.O. and Faeth, G.M., "Spectral Extinction Coefficients of Soot Aggregates From Turbulent Diffusion Flames", *J. Heat Transfer* (ASME) **118** (5) 415-421 (1996)

Koylu, U.O., Xing, Y., and Rosner, D.E.,"Fractal Morphology Analysis of Combustion-Generated Aggregates Using Angular Light Scattering and Electron Microscope Images", *Langmuir* (Amer. Chem. Soc.)**11** (12) 4848-4854 (1995)

Koylu, U. O., "Quantitative Analysis of *In-situ* Optical Diagnostics for Inferring Particle/Aggregate Parameters in Flames: Implications for Soot Surface Growth and Total Emissivity", *Comb & Flame* **109**, 488-500 (1996)

Mackowski, D.W., Tassopoulos, M. and Rosner, D.E.,"Effect of Radiative Heat Transfer on the Coagulation Dynamics of Combustion-Generated Particles", *Aerosol Sci. Technol.(AAAR)* **20** (1) 83-99, (1994))

McEnally, C.S.,and Pfefferle, L.D(1997),"Experimental Assessment of Napthalene Formation Mechanisms in Non-Pre-mixed Flames", *Comb. Sci. Tech.* **128** 257-278

Neimark, A.V., Koylu, U. O., and Rosner, D.E., "Extended Characterization of Combustion-Generated Aggregates: Self-Affinity and Lacunarities", *J. Colloid Int. Sci.*,**180**, 590-597(1996)

Rosner, D.E.(1997) "Combustion Synthesis and Materials Processing",, *Chemical Engineering Education* (ASEE), Fall 1997 Graduate Issue **31** (4) 228-235 (November 1997); Student Exercises: *loc. cit.* **32**(1), 82-83(1998)

Rosner, D.E. and Kim, S.S., "Optical Experiments on Thermophoretically Augmented Submicron Particle Deposition From 'Dusty' High Temperature Gas Flows", *Chemical Engrg. J.*(Elsevier) **29**,[3], 147-157 (1984)

Rosner, D.E. and Nagarajan, R.,"Toward a Mechanistic Theory of Net Deposit Growth from Ash-Laden Flowing Combustion Gases: Self-Regulated Sticking of Impacting Particles and Deposit Erosion in the Presence of Vapor 'Glue'", *Proc. 24th National Heat Transfer Conf.*, AIChE Symposium Series, Vol. **83** [257], 289-296, (1987)

Rosner, D.E., Chen, B.K., Fryburg, G.C. and Kohl, F.J., "Chemically Frozen Multicomponent Boundary Layer Theory of Salt and/or Ash Deposition Rates from Combustion Gases", *Comb Sci & Tech* **20**, 87-106 (1979)

Rosner, D.E., **Transport Processes in Chemically Reacting Flow Systems**, Butterworth-Heinemann, Stoneham MA, 1986; 3d Printing 1990.

Rosner, D.E. and Tandon, P., "Prediction and Correlation of 'Accessible' Area of Large Multi-particle Aggregates ", *AIChE J.* **40** (7), 1167-1182 (1994)

Rosner, D.E., Tandon, P. and Konstandopoulos, A.G., "Rational Prediction of Inertially Induced Particle Deposition Rates for a Cylindrical Target in Dust-Laden Streams", *Proc. 1st Int. Particle Technology Forum*, AIChE , **Vol. II**, 374-381 (1994).

Rosner, D.E., Mackowski, D.W and Garcia-Ybarra, P., "Size and Structure-Insensitivity of the Thermophoretic Transport of Aggregated 'Soot' Particles in Gases", *Comb. Sci & Tech* **80** (1-3), 87-101 (1991).

Rosner, D.E. and Tassopoulos, M.(1991), "Direct Solutions to the Canonical 'Inverse' Problem of Aerosol Sampling Theory: Coagulation and Size-dependent Wall Loss Corrections for Log-Normally Distributed Aerosols in Upstream Sampling Tubes", *J. Aerosol Sci.* **22** (7) 843-867 (1991).

Rosner, D.E., Mackowski, D.W,. Tassopoulos, M., Castillo, J.L., and Garcia-Ybarra, P., "Effects of Heat Transfer on the Dynamics and Transport of Small Particles in Gases", *I/EC-Research (ACS)* **31**, 760-769 (1992)

Rosner, D. E., Tandon, P. , and Labowsky, M.J. (1995), "Rapid Estimation of Cylinder Erosion Rates in Abrasive Dust-Laden Streams: Effects of Erosion Rate Law and Dust Polydispersity on Predicted Local and Total Target Wear", *AIChE J.*,**41**(5) 1081-1098

Rosner, D.E., Konstandopoulos, A.G., Tassopoulos, M., and Mackowski, D.W (1992), "Deposition Dynamics of Combustion-Generated Particles: Summary of Recent Studies of Particle Transport Mechanisms, Capture Rates, and Resulting Deposit Microstructure/Properties", *Proc. Eng. Foundation Conf* **Inorganic Transformations and Ash Deposition During Combustion**, Engrg. Foundation/ASME, NYC; pp. 585-606

Rosner, D.E., Khalil, Y.F. and Tandon, P., (1996) "Prediction/Correlation of Erosion Rates and Shape Evolution for Ceramic Surfaces Exposed to Flows of Abrasive Suspensions", Proc. *Fifth World Congress of Chemical Engineering*, AIChE, San Diego,CA, July 14-18, 1996 Paper #112e , Vol. **IV**, 1013-1018

Rosner, D.E. and Tandon, P.(1995), "Rational Prediction of Inertially Induced Particle *Deposition* Rates for Cylindrical Target in Dust-Laden Stream" *Chem Eng. Sci.* **50** (21) 3409-3431

Rosner, D. E., Tandon, A.G., and Konstandopoulos, A.G.(1995), "Local Size Distributions of Particles Deposited by Inertial Impaction on a Cylindrical Target in Dust-Laden Streams", *J. Aerosol Sci.*,(Pergamon) **26** (8) 1257-1279

Roth, P. and Fillippov, A.V.(1996), "*In Situ* Ultra-fine Particle Sizing by a Combination of Pulsed Laser Heat-up and Particle Thermal Emission",*J. Aerosol Sci.*, **27** 95-104

Tandon, P., and Rosner, D. E., "Co-deposition on Hot CVD Surfaces: Particle Dynamics and Deposit Roughness Interactions", *AIChE J.* **42** (6) 1673-1684 (1996)

Tandon P., **Transport Theory for Particles Generated in Combustion Environments** PhD Dissertation, Yale University-Graduate School, Dept. Chemical Engineering, May 1995

Tandon, P., and Rosner, D.E. (1996),"Sintering Kinetics and Transport Property Evolution of Large Multi-Particle Aggregates", *Chem. Eng. Communic.* , **151**, 147-168

Xing, Y., Köylü Ü. Ö., Tandon P. and Rosner D. E.(1996), "Measuring and Modeling the Synthesis and Morphological Evolution of Particles in Counterflow Diffusion Flames", Proc. *Fifth World Congress of Chemical Engineering*, AIChE, San Diego, CA, July 14-18, 1996 Paper #88d, Vol. V, pp 43-48.

5.2 PUBLICATIONS WHICH APPEARED BASED ON GRANT AFOSR 97-1-0266

Filippov, A.V, and Rosner, D.E.,(1999)."Energy Transfer Between an Aerosol Particle and Gas at High Temperature Ratios in the Knudsen Transition Regime", *Int. J. Heat Mass Transfer* **43** ,127-138 (2000)

Filippov, A.V., Rosner, D.E (1998), "Particle-to-Gas Energy Transfer During Laser-Induced Incandescence", *J. Aerosol Sci.*(Elsevier) **29** , Suppl. 1, S583-S584,

Garcia-Ybarra, P. and Castillo, J.L.(1998) "Asymptotic Analysis of the Drag on a Porous Sphere", *J. Aerosol Sci.*(Elsevier) **29** , Suppl. 1, pp. S1069-S1070

Koylu, U. O., McEnally, C.S., Rosner, D.E., and Pfefferle, L.D., "Simultaneous Measurements of Soot Volume Fraction and Particle Size/Microstructure in Flames Using a Thermophoretic Sampling Technique", *Comb & Flame* **110** (4) 494-507 (1997)

McEnally, C.S., Koylu, U.O., Pfefferle, L.D. and Rosner, D.E., "Soot Volume Fraction and Temperature Measurements in Laminar Non-Premixed Flames Using Thermocouples", *Comb & Flame* **109** 701-720(1997)

McEnally, C.S., Koylu, U.O., Pfefferle, L.D. and Rosner, D.E., "Soot Volume Fraction and Temperature Measurements in Laminar Non-Premixed Flames Using Thermocouples", *Comb & Flame* **109** 701-720(1997)

Rosner, D.E., "Knudsen Transition Effects on Total Mass Deposition Rates From 'Coagulation-Aged Aerosol Populations", AIChE-*Particle Technology Forum*, in Vol **1**, **Advanced Technologies for Particle Processing**, AIChE/IChE, pp. 357-362, November 1998

Rosner, D.E.(1997) "Combustion Synthesis and Materials Processing", *Chemical Engineering Education* (ASEE), Fall 1997 Graduate Issue **31** (4) 228-235 (November 1997); Student Exercises: *loc. cit.* **32**(1), 82-83(1998)

Rosner, D.E. and Khalil, Y.F.(1999) ,"Particle Morphology and Knudsen Transition Effects on Thermophoretically Dominated Mass Deposition Rates From 'Coagulation-Aged' Populations", *J. Aerosol Sci* **31** (3) 273-292 .(2000)

Tandon, P., and Rosner, D.E., "Monte-Carlo Simulation of Simultaneous Particle Aggregation and Simultaneous Restructuring", *J Colloid Interface Sci.* **213**, 273-286 (1999)

Xing, Y., Rosner, D.E., Koylu, U.O. and Tandon, P.(1997) "Morphological Evolution of Oxide Nano-particles in Laminar Counterflow Diffusion Flames---Measurements and Modelling", *AIChE J.* (Special Issue on Ceramics Processing) **43** (11A) 2641-2649

Xing, Y., Koylu, U O and Rosner, D E,"*In situ* Light Scattering Measurements of Morphologically Evolving Flame-Synthesized Oxide Nano-Aggregates", *Applied Optics* **38** (12) 2686-2697(1999)

Xing, Y. and Rosner, D.E. (1999) "Prediction of Spherule Size in Gas Phase Nano-Particle Synthesis", Invited Paper for *J. Nanoparticle Research*, Special Issue on *Vapor Phase Synthesis of Nano-particles* **1** ,277-291(1999)

Xing, Y., **Synthesis and Morphological Evolution of Inorganic Nano-particles in Gas Phase Flames**, PhD Dissertation, Yale University Graduate School, Chemical Engineering Dept., December 1997

Xing, Y., **Synthesis and Morphological Evolution of Inorganic Nano-particles in Gas Phase Flames**, PhD Dissertation, Yale University Graduate School, Chemical Engineering Dept., December 1997

5.3 PUBLICATIONS SUBMITTED/IN PRESS BASED ON GRANT AFOSR 97-1-0266

Filippov, A.V, Rosner, D.E. and Kumar M. (1999) "When and How Can LII be Used to Determine Soot Aggregate Size Distributions?", Paper 142, Session B-4, 1999 Joint Technical Mtg.-Combustion Inst.; *Comb Sci & Tech* (submitted, April, 1999; in press, 2000)

Filippov, A.V.(1999), "Theory of Hydrodynamic Interaction of N Arbitrary Spheres at Low Reynolds Number", *J. Colloid Interface Sci* (in press,2000)

Rosner, D.E. and Yu, S., "Monte-Carlo Simulation of Free-Molecule Regime Brownian Aggregation and Simultaneous Spheroidization", *AIChE J.* (submitted, May 1999; revision in preparation)

LIST OF ABBREVIATIONS

ALS	Angular Light Scattering	BL	Boundary layer
CDF	Counterflow diffusion flame	TEM	Transmission Electron Microscopy
CVD	Chemical vapor deposition	CRF	Combustion Research Facility
D_f	Fractal dimension	GRA	Graduate research Asst.
G/S	Gas/solid interface	JTPV	"Jump" Thermophoretic Velocimetry
LDV	Laser Doppler Velocimetry	LII	Laser-induced incandescence
LLS	Laser light scattering	LTCE	local thermochem. equilibrium
PBE	Population Balance Eq.	*pdf*	Probability density function
PI	Principal Investigator	PSD	Particle size distribution
MRS	Materials Research Society	TMA	Trimethyl aluminum
VS	Visiting Scholar	TPD	Thermocouple Particle Densitometry
TSPD	Thermophoretic sampling particle diagnostic		
TPV	Thermophoretic velocimetry		

*Full-length reprints previously unavailable are reproduced in Section 6 (along with Forms 298)

6. APPENDICES (Complete Previously Unreported Papers on GRANT AFOSR 97-1-0266; including Form 298 for each)

PIADC Survey INFO (*cf.* Sections 5.2, 6):

PI DATA

Name: Daniel E. Rosner

Institution: Yale University

Contract/Grant No.: AFOSR 97-1-0266

NUMBER OF GRANT CO-INVESTIGATORS

Fac. 1 **Post-docs.** 2 **Grad Students** 2 **Other** 1

PUBLICATIONS RELATED TO AFOREMENTIONED GRANT

Name of Journal: *J. Nanoparticle Research*, (Special Issue on *Vapor Phase Synthesis of Nano-particles)*

Title of (Invited) Article: "Prediction of Spherule Size in Gas Phase Nano-Particle Synthesis

Authors: Xing, Y. and Rosner, D. E.

Publisher: Kluwer

Volume: **1** Pages: 277-29 Month Published: July(?) Year: (1999)

Name of Journal: *J. Aerosol Sci*

Title of Article: "Particle Morphology and Knudsen Transition Effects on Thermophoretically Dominated Mass Deposition Rates From 'Coagulation-Aged' Populations"

Authors: Rosner, D. E. and Khalil, Y.F.

Publisher: Elsevier

Volume: **31** Pages: 273-292 Month Published: March Year: (2000)

HONORS/AWARDS RECEIVED: ***Senior Scientist Research Award of the AAAR***

Professor **Daniel E. Rosner** of the Yale *Department of Chemical Engineering* , has just been named as the 1999 D. Sinclair Award Winner of the *American Association of Aerosol Research* (AAAR). Presented October 13, 1999 in Tacoma WA at the 18th Annual Mtg. of AAAR, a society devoted to the science and technology of gas-borne particulate matter, this award recognizes sustained excellence in aerosol research and technology by an established scientist. Professor Rosner, who joined the Yale ChE Faculty in 1969 after 10 years of industrial research experience, is the author of over 230 research publications, many dealing with the synthesis, coagulation, restructuring kinetics, transport properties, and detection/characterization of gas-borne particles, often with dimensions as small as 10 nanometers. Such particles are important in air pollution control engineering and semi-conductor processing, as well as the industrial scale production of high-value ultra-fine powders, pigments, and optical wave guide fibers.

REPORT DOCUMENTATION PAGE

Form Approved
OMB No. 0704-0188

1. AGENCY USE ONLY (Leave blank)	2. REPORT DATE	3. REPORT TYPE AND DATES COVERED
	Summer 1999	Reprint

4. TITLE AND SUBTITLE

(U) Prediction of spherule size in gas phase nanoparticle synthesis

5. FUNDING NUMBERS

PE - 61102F
PR - 2308
SA - BS
G-F49620-97-1-0266

6. AUTHOR(S)

Yangchuan Xing and Daniel E. Rosner

7. PERFORMING ORGANIZATION NAME(S) AND ADDRESS(ES)

Yale University
High Temperature Chemical Reaction Engineering Laboratory
Department of Chemical Engineering
PO Box 208286 YS, New Haven, CT 06520-8286 USA

8. PERFORMING ORGANIZATION REPORT NUMBER

9. SPONSORING/MONITORING AGENCY NAME(S) AND ADDRESS(ES)

AFOSR/NA
801 N Randolph St., Rm. 732
Arlington VA 22203-1977

10. SPONSORING/MONITORING AGENCY REPORT NUMBER

11. SUPPLEMENTARY NOTES

Journal of Nanoparticle Research 1: 277–291, 1999.

12a. DISTRIBUTION/AVAILABILITY STATEMENT

Approved for public release; distribution is unlimited

12b. DISTRIBUTION CODE

13. ABSTRACT (Maximum 200 words)

Surprisingly, there is still no rational yet practical method to reliably predict absolute 'primary' nanospherule sizes and, hence, specific surface areas, in gas phase flame nanoparticle synthesis. The present paper summarizes our approach to this important problem, using a plausible and tractable coagulation–coalescence (two-rate process) model, but with an important modification to the rate of nanoparticle coalescence. The Smoluchowski equation is used to describe the particle Brownian coagulation rate process (free-molecule regime), together with the assumption that the particle population follows a self-preserving size distribution. The decisive coalescence process, driven by the minimization of surface energy of the coalescing nanoparticles, is presumed to occur *via* the mechanism of surface diffusion. However, a curvature-dependent energy barrier for surface-diffusion is proposed, taking into account the extended 'surface-melting' behavior of nanoparticles. This is shown here to have the effect of accelerating the coalescence rate of touching nanoparticles, leading to absolute sizes (at the predicted onset of aggregate formation) in encouraging agreement with available experiments. It was found that the coalescence rate, especially with a curvature-augmented surface diffusivity, is far more sensitive to particle size than is the Brownian coagulation rate. As a result, when cast in terms of characteristic process times, a distinct crossover generally exists, allowing the determination of observed 'primary' spherule sizes within larger aggregates. This approach is successfully applied here to several published synthesis examples of vapor-derived nanosized alumina and titania. Its broader implications for nanoparticle synthesis in non-isothermal reactors, including our own counterflow diffusion flame reactor, are also briefly summarized.

14. SUBJECT TERMS

Laser-induced incandescence. soot morphology , aggregated particles, particle mass transport thermophoresis, Brownian diffusion, particle sampling, nano-particle formation/restructuring in flames, deposition rate theory

15. NUMBER OF PAGES

15

16. PRICE CODE

17. SECURITY CLASSIFICATION OF REPORT	18. SECURITY CLASSIFICATION OF THIS PAGE	19. SECURITY CLASSIFICATION OF ABSTRACT	20. LIMITATION OF ABSTRACT
Unclassified	Unclassified	Unclassified	UL

Journal of Nanoparticle Research **1**: 277–291, 1999.

Prediction of spherule size in gas phase nanoparticle synthesis*

Yangchuan Xing** and Daniel E. Rosner***
*Department of Chemical Engineering, High Temperature Chemical Reaction Engineering Laboratory, Yale University, New Haven, CT 06520-8286, USA; **Present address: Department of Chemical Engineering, Johns Hopkins University, Baltimore, MD 21218 (E-mail: yangchuan.xing@jhu.edu); ***Author for correspondence (E-mail: daniel.rosner@yale.edu)*

Received 1 December 1998; accepted in revised form 14 March 1999

Key words: nanoparticles, specific surface area, surface melting, coalescence, surface diffusion, flame particle synthesis

Abstract

Surprisingly, there is still no rational yet practical method to reliably predict absolute 'primary' nanospherule sizes and, hence, specific surface areas, in gas phase flame nanoparticle synthesis. The present paper summarizes our approach to this important problem, using a plausible and tractable coagulation–coalescence (two-rate process) model, but with an important modification to the rate of nanoparticle coalescence. The Smoluchowski equation is used to describe the particle Brownian coagulation rate process (free-molecule regime), together with the assumption that the particle population follows a self-preserving size distribution. The decisive coalescence process, driven by the minimization of surface energy of the coalescing nanoparticles, is presumed to occur *via* the mechanism of surface diffusion. However, a curvature-dependent energy barrier for surface-diffusion is proposed, taking into account the extended 'surface-melting' behavior of nanoparticles. This is shown here to have the effect of accelerating the coalescence rate of touching nanoparticles, leading to absolute sizes (at the predicted onset of aggregate formation) in encouraging agreement with available experiments. It was found that the coalescence rate, especially with a curvature-augmented surface diffusivity, is far more sensitive to particle size than is the Brownian coagulation rate. As a result, when cast in terms of characteristic process times, a distinct crossover generally exists, allowing the determination of observed 'primary' spherule sizes within larger aggregates. This approach is successfully applied here to several published synthesis examples of vapor-derived nanosized alumina and titania. Its broader implications for nanoparticle synthesis in non-isothermal reactors, including our own counterflow diffusion flame reactor, are also briefly summarized.

1. Introduction

Aerosol processes for producing ultrafine inorganic particles have a long history, especially the use of gas phase flames to synthesize pigments (e.g. TiO_2), which can be traced back roughly half of a century. Flame processes are still widespread in industry to economically generate fine powders, including non-pigmentary applications in which the premium is placed on specific surface area rather than visible light scattering power. Unfortunately, the fundamentals of particle formation in such environments are not well understood, especially particle growth kinetics in the early 'nanoparticle' formation stages. This is partly due to the fact that processes at these early stages are extremely fast (Pratsinis, 1998), mostly taking place

*Invited paper

on a sub-millisecond time scale. Additionally, physicochemical properties of particles on the nanometer scale are still not well documented.

In earlier laboratory studies of flame-synthesized powders, Ulrich and co-workers (Ulrich, 1971; Ulrich & Subramanian, 1977) attempted to predict silica spherule size in laminar and turbulent flames. In their seminal work, they suggested that Brownian coagulation and coalescence were the rate processes determining observed particle size and morphology, with growth from the vapor phase (CVD or vapor condensation) playing a secondary role. In their work, particle formation was simply interpreted as resulting from coagulation, followed by rapid coalescence as a result of surface-energy driven viscous flow. Semiquantitative comparison with experiments revealed some discrepancies, attributed to inaccuracies of available experimental measurements. In a more recent study, Koch & Friedlander (1990a) have suggested a convenient, asymptotically valid form for aggregate sintering rate in terms of surface areas. In their work a characteristic coalescence time was introduced, expressed in multiples of the 'monomer particle' sintering time. The latter was based on the sintering of spherical particles *via* viscous flow or solid-state diffusion. Other studies (Lehtinen et al., 1996a,b; Koch & Friedlander, 1990b; Tandon & Rosner, 1996; Flagan & Luden, 1995; Kruis et al., 1993; Helble & Sarofim, 1989) were principally concerned with the primary particle growth by sintering within aggregates, in which two or more constituent spherules (adjacent 'primary' particles) sinter together. Typically, in all of these studies, it has been assumed, either explicitly or implicitly, that macroscopic material properties can be applied to nanoparticles. While this can be valid for large particles (often >50 nm and depending on material), for much smaller particles (ca. 10 nm) this assumption can evidently result in large errors in the predicted coalescence rate (Wu et al., 1993; Xing et al., 1996). Since aerosol particles are necessarily developed from their previous, much smaller 'parent' particles, and must go through a nanoparticle stage, it is very important to understand the coalescence of isolated nanoparticles, before addressing aggregate restructuring. It is now well known that when matter is sufficiently finely divided, especially down to the nanometer scale, many of its physical and chemical properties differ significantly from the corresponding bulk values (see, e.g. Ichinose et al., 1992). Therefore, property changes associated with particle sizes in the nanometer range must be taken into account.

More generally, particle formation from the vapor phase consists of four basic steps, not necessarily purely sequential: vapor phase chemical reaction, nucleation of the supersaturated vapor product to form embryonic particles, primary particle growth by vapor condensation and/or heterogeneous chemical reaction, and particle growth as a result of particle–particle collisions, usually associated with their Brownian motion. The rates of these processes can be conveniently ordered in terms of their corresponding characteristic times (Rosner, 1996), and, when compared in this way, there is often only one or two that is rate-controlling step (Xing et al., 1996). Thus, for many metal oxides produced in flames (e.g. Al_2O_3, TiO_2, and SiO_2) it is found that their critical nucleus radii, formally calculated from the Gibbs–Kelvin equation, are of the order of their molecular radii. This follows from the smallness of the oxide equilibrium vapor pressure at the temperature at which the oxide vapor is chemically produced. For example, the equilibrium vapor pressure of alumina at 1000 K is approximately 10^{-14} Pa, but the vapor pressure for alumina particle formation in laboratory reactors usually exceeds 10 Pa. Such high local supersaturation, according to classical nucleation theory, easily makes every product molecule, here Al_2O_3(g), a 'stable nucleus'. In such cases, as a useful sol reaction engineering (SRE) simplification, particle 'nucleation' may be considered virtually instantaneous, and explicitly neglected (Ulrich, 1971). Therefore, if the vapor precursor does not chemically persist, particle growth in such environments can be regarded as the result of (post-reaction) physical coagulation and coalescence processes. Conditions for the validity of this idealized two-rate process model are easily satisfied if the precursor vapor reaction (often hydrolysis) is sufficiently fast, which is true for many metal oxide precursors in current use, especially organometallic molecules (Xing et al., 1996).

Adopting this two-process picture, and following Ulrich (1971), and Koch & Friedlander (1990a), in Section 2, we apply the Smoluchowski coagulation rate equation in a non-isothermal environment representative of a wide variety of aerosol synthesis processes. To more accurately describe the observed coalescence rate of nanoparticles, we introduce a microscopic but quasi-continuum model based on the 'surface melting concept' (Section 2.3). This concept leads us to a curvature-dependent and significantly enhanced surface self-diffusion coefficient for the coalescence of nanoparticles. Moreover, at the prevailing temperatures we show that the coalescence rate associated with this modified surface diffusivity is much more sensitive to particle size than is the Brownian coagulation rate. Therefore, a distinct 'crossover' generally exists between the two relevant characteristic times as a function of particle size, allowing a determination of the ('primary') spherule size, and this 'crossover size' will often remain 'frozen in'. Specifically, in Section 3.4, predictions using this approach will be shown to be in encouraging agreement with available experimental results on alumina and titania nanoparticles synthesized from several different gas phase flames (Xing et al., 1996; Zhu & Pratsinis, 1996; Rulison et al., 1996), and 'non-flame' aerosol reactors (Okuyama et al., 1989).

2. Theory

2.1. Particle environments of interests

Two canonical classes of environment situation considered here are flames (or other aerosol reactors) which produce a 'cooling' or 'heating' temporal environment as seen by the particle population. Particle evolution in a 'cooling' flame, i.e. one in which the temperature is decreasing with particle residence time, may be divided into three stages, as shown schematically in Figure 1a: (1) coagulation-controlled regime, (2) coalescence-controlled regime, and (3) a (short) transient stage where the coagulation and coalescence times are comparable. In a 'heating' flame environment in which the temperature is increasing with particle residence time (see Figure 1b), particle growth may have one or all of the stages in the 'cooling' case, depending on heating rate and local temperature. If the residence time is long enough, the final product can conceivably be spherical particles because the temperature will ultimately exceed the melting temperature of the particle material, and all aggregates will collapse. For other aerosol reactors, a temperature history can be similarly expressed. Nevertheless, in all cases, there is an initial stage in which the spherules are formed, as illustrated in Figure 1. This stage is characterized by coagulation with instantaneous coalescence, i.e. coagulation-controlled. Because we are interested in rate processes determining nanospherule sizes, the formula below is focused on this stage.

2.2. Brownian coagulation of particle populations

In an isothermal isobaric environment, coagulation of particles (see, e.g. Friedlander, 1977) leads to a decrease in particle number density, while maintaining the condensed phase volume fraction constant. If instantaneous coalescence of the colliding particles is assumed, and particle growth via heterogeneous oxidation of surviving vapor precursor is neglected, the particle production rate can be expressed in terms of the continuous form of the Smoluchowski equation (Friedlander, 1977):

$$\frac{\partial n}{\partial t} = \frac{1}{2}\int_0^{v} \beta(v', v - v')n(v')n(v - v')\,\mathrm{d}v' - \int_0^{\infty} \beta(v', v)n(v')n(v)\,\mathrm{d}v', \quad (1)$$

where $n(v)$ is the number density of particles in the size range $v \pm (1/2)\,\mathrm{d}v$. The collision frequency function appearing in Eq. (1), in the free molecule regime, may be written (Friedlander, 1977):

$$\beta(v, v') = \left(\frac{3}{4\pi}\right)^{1/6} \cdot \left(\frac{6k_B T}{\rho_s}\right)^{1/2} \cdot \left(\frac{1}{v} + \frac{1}{v'}\right)^{1/2} \cdot (v^{1/3} + v'^{1/3})^2, \quad (2)$$

where k_B is the Boltzmann constant, T the temperature, and ρ_s the density of the condensed phase. Since the primary spherules observed in an aerosol process are generally small (less than 50 nm) when compared to the gas mean free path at the synthesis temperature, we only consider this so-called free molecule regime (Eq. 2). The decay in the total number density of particles is obtained by summing Eq. 1 over all particle sizes:

$$\frac{\mathrm{d}N}{\mathrm{d}t} = -\frac{1}{2}\int_0^{\infty}\int_0^{\infty} \beta(v', v)n(v')n(v)\,\mathrm{d}v'\,\mathrm{d}v, \quad (3)$$

where N is the total number of particles per unit volume at (evolution) time t. Introducing a similarity transformation and defining the following 'rescaled' variables (Lai et al., 1972):

$$\eta \equiv v/\bar{v}, \quad \psi(\eta) \equiv n\bar{v}/N, \quad \bar{v} \equiv \phi/N, \quad (4)$$

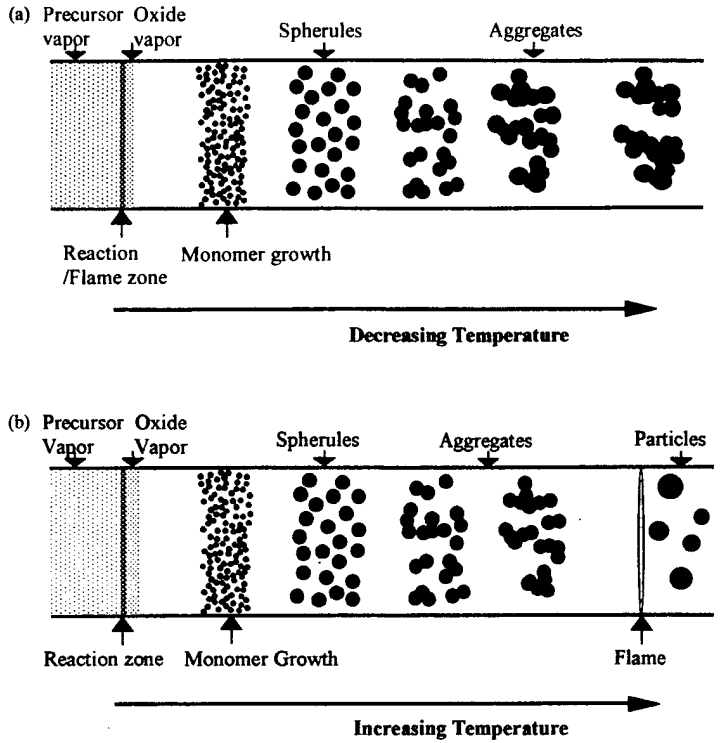

Figure 1. Idealized synthesis flame environments for particle evolution in: (a) 'cooling' flame; (b) 'heating' flame. In both cases the observed particles are isolated and spherical at the initial stages.

where $\bar{v}$ is the average particle volume and ϕ the particle volume fraction, one obtains

$$\frac{dN}{dt} = -\frac{\alpha}{2}\left(\frac{3}{4\pi}\right)^{1/6}\cdot\left(\frac{6k_BT}{\rho_s}\right)^{1/2}\cdot\phi^{1/6}N^{11/6}, \quad (5)$$

where α is the dimensionless collision integral:

$$\alpha \equiv \int_0^\infty\int_0^\infty (\eta^{-1}+\eta'^{-1})^{1/2}(\eta^{1/3}+\eta'^{1/3})^2 \cdot\psi(\eta')\psi(\eta)\,d\eta'\,d\eta, \quad (6)$$

found to be 6.67 by numerical analysis (Friedlander, 1977).

Now consider a non-isothermal flame or aerosol reactor, in which the carrier gas temperature field may be approximated as linear in time (Koch & Friedlander, 1990b), i.e.:

$$T = T_0 + \lambda t, \quad (7)$$

where T_0 is the initial temperature and λ is the heating or cooling rate (negative for cooling and zero for isothermal processes). Since particle volume fraction, ϕ, is not conserved in a non-isothermal isobaric case, it is now convenient to introduce the following parameters expressed in terms of the mass of the gas phase (Wu et al., 1993; Lehtinen et al., 1996a), i.e. the number of particles per unit mass of gas,

$$N_m \equiv \frac{N}{\rho_g} \quad (8a)$$

and the particle volume per unit mass of gas,

$$\phi_m \equiv \frac{\phi}{\rho_g}, \quad (8b)$$

where ρ_g is the gas phase local density. Substituting these relations into Eq. 5 and defining the average particle diameter via

$$\bar{d}_p = \left(\frac{6}{\pi}\bar{v}\right)^{1/3} = \left(\frac{6\phi_m}{\pi N_m}\right)^{1/3}, \quad (9)$$

we obtain the evolution equation:

$$\frac{d\bar{d}_p}{dt} = \left(\frac{\alpha\rho_{g,0}\phi_m}{2\pi}\right)\cdot\left(\frac{12k_BT_0}{\rho_p}\right)^{1/2} \cdot\left(1+\frac{\lambda}{T_0}t\right)^{-1/2}\cdot(\bar{d}_p)^{-3/2} -\left(\frac{\pi\lambda}{18\phi_mT_0}\right)\cdot\left(1+\frac{\lambda}{T_0}t\right)^{-1}\cdot(\bar{d}_p)^4, \quad (10)$$

where use has been made of Eq. (7), $dN_m = (18\phi_m/\pi\bar{d}_p)d(\bar{d}_p)$ and $\rho_g/\rho_{g,0} = T_0/T$ (the ideal gas equation of state). As before, the subscript, 0, refers to the initial state. Note that Eq. (10) contains on the right hand side a term that results from the non-isothermal conditions, i.e. temperature-induced expansion of the local gas phase.

A relaxation time for particle–particle collisions, hereafter called the coagulation time, t_C, can be defined to characterize the coagulation rate process. This characteristic time is (Xing et al., 1996; Friedlander, 1977)

$$t_C = \frac{2}{\beta N}, \quad (11)$$

where from Eq. (2) the value of rate constant β is $\beta(\bar{v},\bar{v})$, or

$$\beta = 4\left(\frac{3}{4\pi}\right)^{1/6}\cdot\left(\frac{12k_BT_0}{\rho_p}\right)^{1/2} \cdot\left(\frac{T}{T_0}\right)^{1/2}\cdot(\bar{v})^{1/6} \quad (12a)$$

and

$$N = \left(\frac{\phi_m}{v}\right)\cdot\left(\frac{T_0}{T}\right)\rho_{g,0}. \quad (12b)$$

2.3. *Surface melting of small particles*

Before we address the coalescence rate and associated characteristic time, it is necessary to develop a microscopic approach to the surface state of small particles. Surface melting of solid has been studied for clusters (Berry, 1997), small particles (Kofman et al., 1994) and flat surfaces (Pluis et al., 1990). Both simulation and experiment have shown that disordering of surface atoms/molecules occurs far ahead of the bulk solid phase at elevated temperatures due to the broken bonds associated with surface atoms (Ichinose et al., 1992; Broughton & Glimer, 1983). Experimental observation also revealed that small particles undergo surface melting process (Chessac et al., 1988), which may lead to near-instantaneous coalescence at low temperatures (Huang et al., 1991).

The thickness of the disordered surface layer, or quasi-liquid layer, can be shown to depend on both particle size and absolute temperature; and the surface melting temperature can be obtained at a fixed thickness of melted-surface layer. In the following we approach this problem through a simple thermodynamic formulation.

The melting temperature, T_{mp}, of a particle of radius r, can be expressed (Couchman & Jesser, 1977),

$$\frac{T_{mp}}{T_{mb}} = 1 - \frac{3}{Lr}\cdot\left[\gamma_{sg} - \gamma_{lg}\left(\frac{\rho_s}{\rho_l}\right)^{2/3}\right], \quad (13)$$

where T_{mb} is the melting temperature of the corresponding bulk solid ($r\to\infty$); L is the latent heat of fusion per unit volume of solid; γ_{sg} and γ_{lg} are surface energies of the solid/gas and liquid/gas interfaces; and ρ_s and ρ_l are the densities of the participating solid and liquid phases. Now consider a particle undergoing the surface melting process, as illustrated in Figure 2. As the temperature is increased, a disordered (melted) surface layer is formed on the particle. Then, the Helmholtz free energy difference per unit area between a surface-melted particle and a particle in the solid state of the same mass can be written (Xing, 1997; Xing & Rosner, 1997):

$$\Delta f = \left(\frac{LT_{mp}r\tau}{3T_{mb}}\right)\cdot(\delta^3-3\delta^2+3\delta)-(1-\Theta) \cdot\left[(\gamma_{sg}-\gamma_{lg})-\gamma_{sl}(1-\delta)^2\right], \quad (14)$$

where $\delta \equiv \xi/r$ is a dimensionless length with ξ being the surface liquid layer thickness; $\tau \equiv (T_{mp}-T)/T_{mp}$

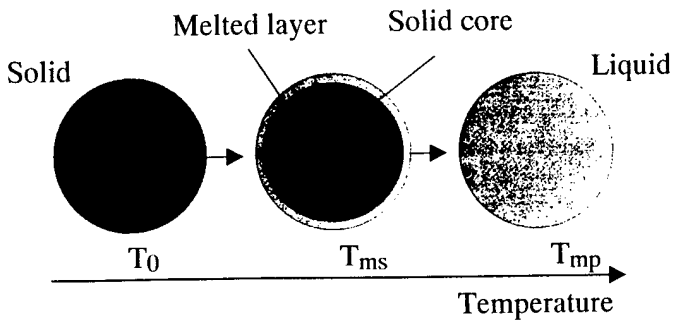

Figure 2. Schematic diagram of the surface melting processes. A particle is considered solid at 0 K and liquid at its melting temperature, T_{mp}. For intermediate temperatures, the particle is considered in a 'surface melted' state.

is a dimensionless temperature; and

$$\Theta = \exp\left[-\frac{\xi}{(1-\delta)\zeta}\right] = \begin{cases} 1, & \text{for a solid surface,} \\ 0, & \text{for a liquid surface,} \end{cases} \tag{15}$$

is the surface order parameter with ζ being the liquid correlation length (Van de Veen et al., 1988; Lowen, 1994). This exponential expression accounts only for short-range interactions, as is suitable for small system (current case). For long-range interactions (van der Waals forces, not considered here) the order parameter has a power law expression (Lowen, 1994). The equilibrium liquid layer thickness at a given temperature T can be obtained by minimizing the free energy difference, i.e. by setting $\partial\Delta f/\partial\xi = 0$ while satisfying the inequality conditions $\partial^2\Delta f/\partial\xi^2 > 0$ and $\Delta f \leq 0$. The surface melting temperature, T_{ms}, of the topmost surface molecules is determined by setting ξ to that surface layer thickness ξ_0, taken as the lattice length of the corresponding material. In Figure 3 we present the surface melting temperature (topmost layer only) calculated from this formulation. The model material considered here is alumina, whose familiar physical properties are listed in Table 1. For comparison, in Figure 3 we also display the particle melting temperature and the bulk melting temperature contours. As anticipated for small particles, the surface melting temperature deviates appreciably from the particle melting temperature, as well as the bulk melting point. The surface melting temperature is lower as the particle size becomes smaller.

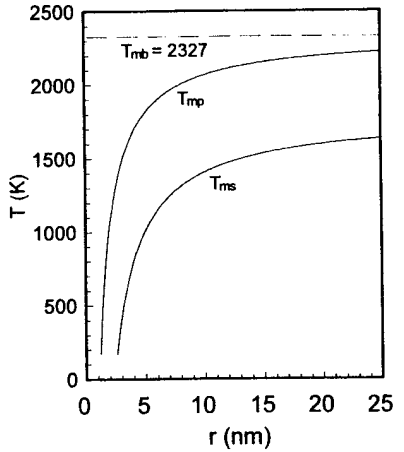

Figure 3. Particle melting temperatures of alumina, showing that the surface melting temperature, T_{ms}, is lower than the particle melting temperature, T_{mp}, which is bounded by the bulk melting temperature (horizontal broken line) T_{mb}.

While we do not expect this quasi-continuum formulation to apply to sizes down to several molecular radii, we believe it will be applicable to many practical systems in which interface curvature effects are important, yet $v/\Omega \gg 1$.

Table 1. Physical properties of alumina and titania used in present calculations

Properties	Alumina		Titania	
ρ_s (kg/m^3)	3970	Lide, 1994	4420	Lide, 1994
T_{mb} (K)	2327	Chase, 1986	2130	Chase, 1986
L (GJ/m^3)	4.32	Lide, 1994	3.70	Lide, 1994
γ_{sg} (J/m^2)	2.3	Mackrodt, 1992	2.14	Oliver et al., 1997
γ_{lg} (J/m^2)	0.70	Samsonov, 1982	0.34	Samsonov, 1982
γ_{sl} (J/m^2)	0.15	Machlin, 1991[a]	0.18	Machlin, 1991[a]
ζ (Å)	7.0	Pluis et al., 1990[a]	8.4	Pluis et al., 1990[a]
ξ_0(Å)	5.13	Lide, 1994	4.58	Lide, 1994
Ω (Å^3)	22	Coblenz et al., 1980	17	Coblenz et al., 1980

[a] Values estimated from the method given in the reference.

2.4. *Coalescence models of spherical particles*

The driving force for coalescence of touching particles is minimization of the surface energy. Four mechanisms have been proposed for the sintering of powders, i.e. viscous flow, evaporation–condensation, volume diffusion and surface diffusion /boundary diffusion.

Only considering condensed phase molecular diffusion, the time for complete coalescence of two spherical particles can be summarized as (Xing et al., 1996; Coblenz et al., 1980)

$$t_S = \frac{k_B T r^a}{c w^b D \Omega \gamma_{sg}}, \tag{16}$$

where w is the surface or grain boundary layer width, Ω is the molecular volume and D is the relevant diffusion coefficient, with the units: m^2/s. The constants are $a = 3, b = 0$ and $c = 120$ for volume diffusion, $a = 4$, $b = 1$ and $c = 225$ for surface diffusion, and $a = 4$, $b = 1$ and $c = 64$ for grain boundary diffusion. This expression is formally extrapolated from the initial sintering rate, with later-stage deviations neglected.

2.5. *Surface melting and associated surface diffusivity*

Although each mechanism can contribute to the ultimate coalescence of particles, many experiments and simulations have demonstrated that surface diffusion is the dominant mechanism for nanoparticles (Bonevich & Marks, 1992; Kusunoki et al., 1993; Zachariah & Carrier, 1994). Since we are dealing with nanoparticles here, only the surface diffusion will be considered below. However, in our discussion, a comparison of the coalescence rates associated with all three mechanisms is given in next section.

The surface self-diffusion coefficient can be generally written (Somorjai, 1994)

$$D_s = D_{s0} \cdot \exp\left(-\frac{E_s}{RT}\right), \tag{17}$$

where E_s is the activation energy for surface diffusion and R the universal gas constant. Experiments have revealed that the activation energy E_s and the prefactor D_{s0} are different at low and high temperatures, generally separated by $T \approx 0.75T_{mb}$ for macroscopic surfaces. It also has been shown that the surface diffusion coefficient can be related to the melting point of the material *via* (Somorjai, 1994; Seebauer & Allen, 1995):

$$D_s = D_{s0} \cdot \exp\left(-\frac{Q_s T_{mb}}{RT}\right), \tag{18}$$

where $Q_s \equiv E_s/T_{mb}$ and has been found to be approximately constant for similar crystalline structure materials (Somorjai, 1994). Equation (18) was obtained from surface diffusion on macroscopic surfaces. For the nanoparticles considered in the present work the surfaces will melt earlier so that T_{mb} now is replaced by the surface melting temperature T_{ms}. If we further postulate that Q_s is explicitly size-independent, then Eq. (18) for small particles becomes

$$D_s(r) \approx D_{s0} \cdot \exp\left(-\frac{Q_s T_{ms}}{RT}\right). \tag{19}$$

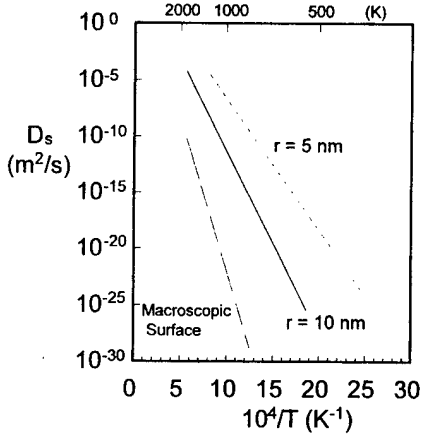

Figure 4. Calculated size-dependent surface diffusion coefficients for alumina nanoparticles. At a given temperature, a remarkable increase in the surface diffusion coefficient is observed for smaller particles.

Since T_{ms} is related to particle size and material properties, we see that the surface diffusion coefficient is curvature-dependent. Equation (19) is the surface diffusion coefficient that will be used in Eq. (16) (for D) for calculating the coalescence characteristic time.

In Figure 4 we plot the corresponding surface self-diffusivity using Eq. (19), together with its macroscopic values (Eq. (18)). We see that the enhancement of the surface diffusion coefficient is significant for small particles. Given a temperature, the ratio can be several decades. Such large diffusion coefficients make it possible for small particles to coalesce 'surprisingly' rapidly (see next section for a quantitative comparison).

3. Results and discussion

3.1. Coagulation of spherical nanoparticles

Coagulation with a self-preserving size distribution has been extensively used to describe particle evolution in flames (Ulrich & Subramanian, 1977; Wu et al., 1993; Matsoukas & Friedlander, 1991). Given Eq. (10) for particle coagulation, it is not difficult to find the isothermal solution by simply setting $\lambda = 0$, leading to the well-known result $\bar{d}_p \sim t^{2/5}$. Equation (10) is a generalized form allowing changes in gas temperature and can be solved for any value of the heating time (λ/T_0^{-1}). In flames of short residence time and small cooling or heating rate, the second term in Eq. (10) is much smaller than the first term when particles are small. Therefore, the second term on the right hand side of Eq. (10) can be neglected for nanospherule formation. Integration of Eq. (10) leads to,

$$\bar{d}_p = \left\{ \left(\frac{5\alpha\rho_{g,0}\phi_m T_0}{2\pi\lambda} \right) \cdot \left(\frac{12 k_B T_0}{\rho_s} \right)^{1/2} \cdot \left[\left(\frac{T}{T_0} \right)^{1/2} - 1 \right] + (\bar{d}_{p,0})^{5/2} \right\}^{2/5}, \tag{20}$$

or explicitly in time:

$$\bar{d}_p = \left\{ \left(\frac{5\alpha\rho_{g,0}\phi_m T_0}{2\pi\lambda} \right) \cdot \left(\frac{12 k_B T_0}{\rho_s} \right)^{1/2} \cdot \left[\left(1 + \frac{\lambda}{T_0} t \right)^{1/2} - 1 \right] + (\bar{d}_{p,0})^{5/2} \right\}^{2/5}. \tag{21}$$

For purposes of discussion, alumina was used in our calculations because of its well-known physical properties (see Table 1) and the availability of aerosol evolution measurements (Xing et al., 1999). In Figure 5 we plot the results for the coagulation of nanoparticles starting from molecular monomers. As is seen, particle growth is directly related to the precursor loading and initial temperature. Additionally residence time has a more pronounced effect on particle size in high temperature-gradient flames than in an isothermal environment. However, for the short residence times considered here the calculated results show only a small deviation, as illustrated in Figure 5. The small deviation is due to the slow cooling/heating rates and short residence time, since under these conditions we can approximate the time term as: $(1 + \lambda t/T_0)^{1/2} - 1 \approx \lambda t/(2T_0)$. But as the particles grow larger the deviation becomes larger, and the higher order terms can no longer be neglected. The effects of the particle loading can also be seen in Figure 5, which shows that higher loading leads to larger particles at the same residence time.

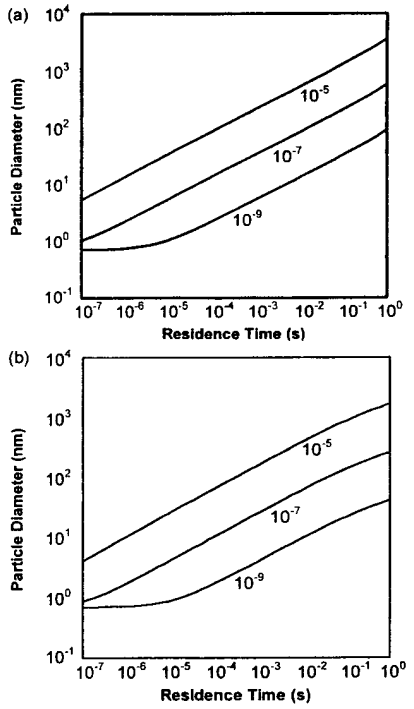

Figure 5. Predicted particle growth due to coagulation with instantaneous coalescence in cooling flame (a) $T_0 = 1500$ K and $\lambda = -10^3$ K/s, and heating flame (b) $T_0 = 500$ K and $\lambda = 10^4$ K/s. The three particle loadings indicated in the figures are in unit m^3/kg.

3.2. Coalescence of spherical nanoparticles

We begin our discussion of the coalescence of nanoparticles with an overview on why sintering models using macroscopic properties necessarily fail for nanoparticle formation from the gas phase. We first compare the coalescence time for two touching particles via three of the sintering mechanisms, i.e. volume diffusion, grain boundary diffusion and surface diffusion (see last section). Using alumina and titania as model materials (see Table 1 and Table 2 for their physical properties), we calculate the coalescence times for spherical particles of radius of 5 and 10 nm at temperature, for example, 800 K. The results are assembled in Table 3. We see that the coalescence times obtained from the macroscopic model can be as long as months or even years for these nanoparticles, whereas in real situation, the residence time and the coagulation time are much shorter (ca. ms). Therefore, if particle coalescence were governed by these macroscopic properties, nanoparticles would never coalesce in the available residence time. This contradicts the experimental results, in which spherules of several tens of nanometers have been synthesized.

Using the surface curvature-dependent diffusivity, Eq. (19), we obtain the results plotted in Figure 6. Within the size range under consideration, we find that the coalescence times are many orders of magnitude smaller than those obtained from using bulk properties. Such dramatic changes make it possible to sinter particles of up to tens of nanometers in a much shorter time (ca. 1 μs). The sharp decrease of coalescence time results from the decrease in particle size.

Table 2. Diffusion coefficients[a] and activation energies for surface diffusion (s), grain boundary diffusion (b) and volume diffusion (v) of alumina and titania

Properties	Alumina		Titania	
E_s (kJ/mol)	518	Seebauer & Allen, 1995	284	Astier & Vergnon, 1976
D_{s0} (m^2/s)	1.0×10^5	Seebauer & Allen, 1995	3.6×10^{-5}	Astier & Vergnon, 1976
E_b (kJ/mol)	418	Wu et al., 1993	258	Astier & Vergnon, 1976
D_{b0} (m^2/s)	0.86	Wu et al., 1993	1.6×10^{-5}	Astier & Vergnon, 1976
E_v (kJ/mol)	577	Wu et al., 1993	313	Astier & Vergnon, 1976
D_{v0} (m^2/s)	1.36×10^5	Wu et al., 1993	4.5×10^{-4}	Astier & Vergnon, 1976

[a]The diffusion layer width is assumed to be 1 nm (Coblenz et al., 1980).

Table 3. Order of magnitude comparison of time scales using macroscopic properties for different sintering mechanisms: Volume diffusion, grain boundary diffusion and surface diffusion ($T = 800$ K)

	Particle radius (nm)	Volume t_v (ms)	Grain boundary t_b (ms)	Surface t_s (ms)
Al_2O_3	5	10^{17}	10^{14}	10^{14}
	10	10^{18}	10^{16}	10^{16}
TiO_2	5	10^{9}	10^{8}	10^{8}
	10	10^{10}	10^{10}	10^{10}

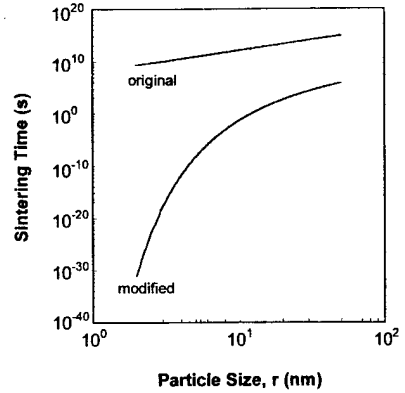

Figure 6. Comparison of sintering times at 800 K for different particle sizes using the original surface diffusivity (Eq. (18)) and the modified diffusivity (Eq. (19)). A significant decrease in sintering time is observed using the curvature-dependent diffusion coefficient.

3.3. *Predicting spherule sizes in flame particle synthesis: General cases*

The particle size evolution by coagulation with the collision frequency function expressed in Eq. (2) is based on the important assumption that the coalescence rate is 'instantaneous'. This assumption has been effectively used in aerosol evolution situations when the particles are sufficiently small. However, as the particles grow larger, this assumption fails, since the particle coalescence rate is no longer 'instantaneous'. Indeed, aggregates consisting of many spherules (or 'primary' particles) are commonly observed in experiments. Thus, we seek the point where particles stop growing under the prevailing conditions. Beyond this point spherule growth will effectively stop and 'fractal-like' aggregates will be formed. As also emphasized in the work of Lehtinen et al. (1996a) and Xing et al. (1996), this point is actually the crossover between the characteristic coagulation and coalescence times.

We begin with a synthesis environment with decreasing temperature, i.e. λ in Eq. (7) is negative. Particle evolution in such case has been illustrated in Figure 1a. In Figure 7 the influence of initial temperature on particle size is shown, where the characteristic times (coagulation and coalescence) are plotted against particle size on a logarithmic scale. We see that the coagulation time is much longer than the coalescence time at small particle size, but the coalescence time quickly increases, as the particles grow. Because the slopes of the curves differ significantly at the crossover (note the log scales), i.e. $dt_s/d(\bar{d}_p) \gg dt_c/d(\bar{d}_p)$, particle growth by coalescence effectively 'stops' beyond this crossover, after which the aggregates, not single particles, are expected. This 'stop' particle size would be the spherule size observed in experiments. From Figure 7 we see that an increase of the initial temperature from 1000 to 2000 K leads to an increase in particle diameters approximately from 30 to 400 nm, showing a significant effect of temperature.

Results at different particle loadings (10^{-5}, 10^{-7} and 10^{-9} m^3/kg-gas) are presented in Figure 8, roughly corresponding to the loading ranges in most laboratory experiments. Under conditions of an initial temperature 1500 K and a cooling rate 10^3 K/s, the spherule diameters are calculated to be 590, 270 and 58 nm, respectively. The loading of 10^{-5} m^3/kg-gas is also comparable to the industrial loading in the lower range, and we see that this loading produces a particle size also comparable to those found in commercial pigmentary powders (ca. 0.5–1 μm). Cooling rates are generally limited by flame conditions, and are found to have little apparent effects on spherule size because of the much higher rates of coagulation and coalescence.

Heating flames are modeled as shown in Figure 1b, where the counterflow diffusion flame reactor is taken as a prototypical case (Xing et al., 1996). Under the conditions $T_0 = 500$ K and $\lambda = 10^4$ K/s, close to that achieved in our experiment (Xing et al., 1996), we have calculated the effect of loading level on particle size. These results are presented in Figure 9. Unlike cooling flames, in which particles are formed in the high temperature region, the reaction of precursors (e.g., trimethylaluminum for alumina) in a heating flame can occur at a much lower temperature. Therefore, spherule diameters (7.7 and 8.3 nm, in Figure 9) are generally smaller than those found in cooling flames.

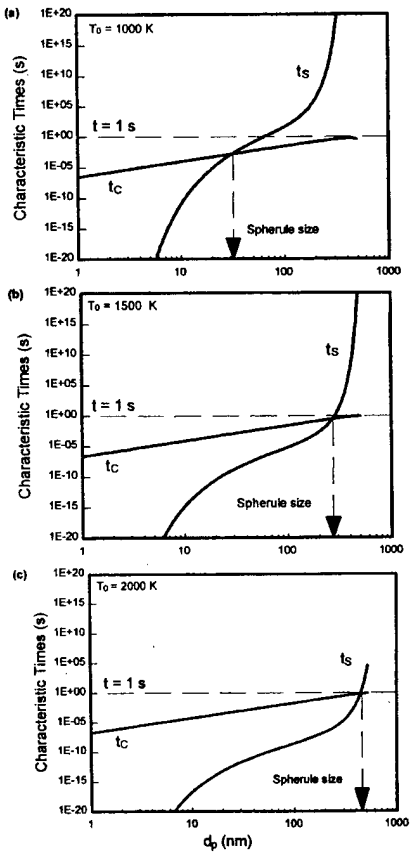

Figure 7. Initial temperature effects on the spherule sizes in a cooling flame with $\phi_m = 10^{-7}$ m^3/kg, showing the increase of 'crossover' particle size with initial temperature T_0: a factor of 2 increase in T_0 results in more than 10 fold increase in particle diameters. The horizontal dotted line corresponds to time scale 1 s, and an arrow indicates the crossover spherule size.

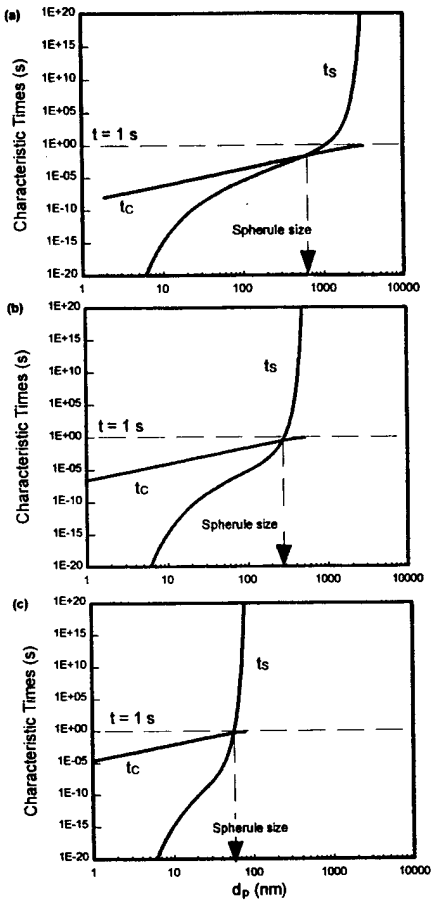

Figure 8. Particle loading effects on crossover spherule sizes in a cooling flame at $T_0 = 1500$ K and $\lambda = -10^3$ K/s, showing that higher loading leads to larger spherule sizes. (a) $\phi_m = 10^{-5}$ m^3/kg, (b) $\phi_m = 10^{-7}$ m^3/kg, (c) $\phi_m = 10^{-9}$ m^3/kg.

It is interesting to note that, at the lowest considered loading, i.e. 10^{-9} m^3/kg-gas, there is no crossover between the two characteristic times, because at such low loadings, the particle coagulation rate is much

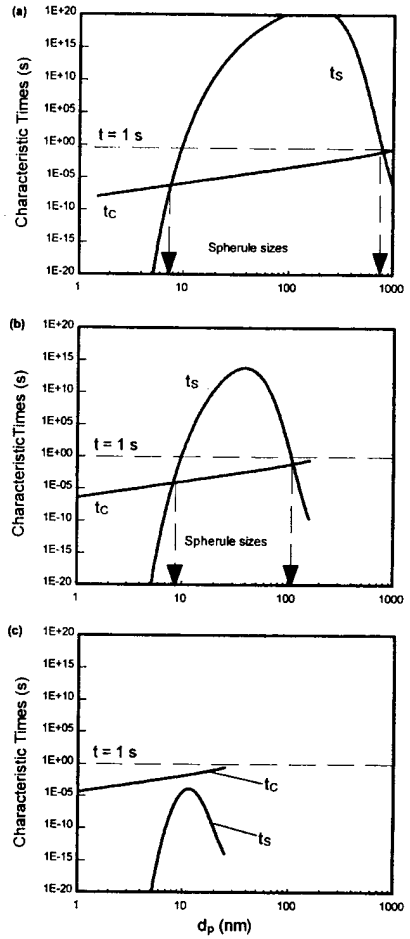

Figure 9. Particle loading effects on the spherule sizes in a heating flame at $T_0 = 500$ K and $\lambda = 10^4$ K/s, showing that higher loading does not necessarily lead to larger spherule size. Also, the coagulation time curve and coalescence time curve may have one, two or no intersection(s). A second crossover is observed at a temperature close to the bulk melting point indicating ultimate collapse of the aggregates. (a) $\phi_m = 10^{-5}$ m^3/kg, (b) $\phi_m = 10^{-7}$ m^3/kg, (c) $\phi_m = 10^{-9}$ m^3/kg.

slower than the heating rate. Therefore, at any time, particles are small enough to coalesce instantaneously and always exist as isolated spherical particles. The evolution of particles is entirely controlled by coagulation in this case. On the other hand, for higher loadings in Figure 9, there is a second crossover found in the particle evolution, attributed to high temperatures (close to the bulk melting point) where the aggregates coalesce. This second crossover and its corresponding particle size should approximately correspond to the final particle sizes observed in such flames (refer to Figure 1b). However, since the coalescing particles in this calculation are assumed to be spherical (while they are actually aggregated after the first crossover), there would inevitably be a shift in the location of the second crossover in any real case. Nevertheless, this second crossover reveals a very interesting aspect of particle evolution under heating conditions, which does not appear in cooling flames. While the first crossover sets the spherule size, this second crossover marks the condition where the aggregates would collapse. To determine the second crossover more accurately one needs to address the rate of *aggregate* coagulation and coalescence, topics beyond the scope of this paper. Interested readers may refer to the relevant papers by Tandon and Rosner (1996), Xiong & Pratsinis (1993), Kruis et al. (1993), Seto et al. (1995), Tandon & Rosner (1995), Wu & Friedlander (1993) and Vemury & Pratsinis (1995).

3.4. *Comparison with experimental results*

Having generalized this approach to the prediction of particle size in cooling and heating flames, we are now in a position to apply this approach to real conditions and to compare with available experimental results. We discuss five real experimental cases in the literature (Wu et al., 1993; Xing et al., 1996; Zhu & Pratsinis, 1996; Rulison et al., 1996; Okuyama et al., 1989). Their experimental conditions are summarized in Table 4. The temperature profiles are estimated from the temperature curves given in these papers, while the particle size and loading data are directly given in the papers. Calculated results obtained by the procedures outlined in the last section are presented in Figure 10. Figure 10 is plotted with real particle size against predicted size. In such a way perfect agreement would correspond to the 45° line, above which the experimental size is larger and below which the predicted size is larger. As can be seen, all points are close to this line (as compared

Table 4. Summary of experimental conditions[a] as input in present calculations

Reference	T_0 (K)	λ (K/s)	ϕ_m (m^3/kg)
Okuyama et al. (1989)	773	0	4.97×10^{-7}
Xing et al. (1996)	500	4.5×10^4	2.62×10^{-7}
Wu et al. (1993)	890	-1.08×10^3	6.60×10^{-8}
Zhu & Pratsinis (1996)	1755	-6.0×10^3	2.97×10^{-6}
Rulison et al. (1996)	1000	5.5×10^4	5.67×10^{-7}

[a]If data not directly given, they are estimated from given information.

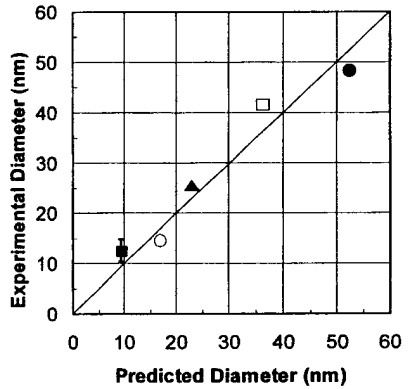

Figure 10. Comparisons of the predicted spherule sizes with available experimental results. ■ – Xing et al. (1996), Al_2O_3; ○ – Okuyama et al. (1989), TiO_2; ▲ – Wu et al. (1993) Al_2O_3; □ – Zhu & Pratsinis (1996), TiO_2; ● – Rulison et al. (1996), TiO_2.

to orders of magnitude differences from classical models), showing that our predictions are in good agreement with available experimental results.

3.5. *Applications and implications*

Characteristic times are useful in describing rate processes in single or multiple phase chemically reacting systems (see, e.g., Rosner, 1986). The characteristic times presented above are just two of the many proposed in a synthesis flame environment (Xing et al., 1996), but in many cases they are the controlling rate processes. Thus, the proposed model is applicable for fast vapor precursor reactions (e.g. $Al(CH_3)_3$, $TiCl_4$) forming low vapor pressure materials (e.g. 'refractory' ceramics such as Al_2O_3, TiO_2, etc.). For high vapor pressure materials like UO_2, evaporation–condensation mechanism may be as important as surface diffusion for the coalescence of small particles, and for slow reactions, heterogeneous processes leading to particle surface growth should be taken into account. Nevertheless, by extending our two-process model, it should be possible to incorporate these and perhaps other complications. For example, nucleation and surface reaction have been incorporated into the coagulation equation, giving rise the so-called 'general dynamic equation' (Pratsinis, 1988). Similarly, the coalescence rate would receive contributions from each of the participating coalescence mechanisms.

Although we have focused on the synthesis of metal oxide particles in this work, the present extended model should also be appropriate for other ceramics formed via any aerosol process, provided the above mentioned assumptions are satisfied. Since surface diffusion has been observed to be the dominant mechanism for the sintering of nanometer particles of most materials, the proposed coalescence model should also find applications in related areas, including nanostructured materials processing, thin film deposition, aerosol evolution and supported-catalyst aging.

4. Conclusions

In this paper, a two-rate process model, describing the competition between Brownian coagulation and surface-energy driven intraparticle coalescence in a non-isothermal environment, has been extended to predict the absolute size of nanometer spherules synthesized via vapor precursors (aerosol processes). The new concept introduced here to predict experimentally observed spherule sizes, and hence specific surface areas, is that of a curvature-dependent energy barrier for surface diffusion, based on a rational microscopic quasi-continuum description of 'surface melting' and its consequences. For simplicity, and because of a lack of chemical kinetic information relevant to such nanoparticle surfaces, we have neglected the possibility of subsequent nanoparticle growth via the heterogeneous oxidation of 'surviving' vapor precursor (Pratsinis & Spicer, 1998).

Our transient one-dimensional calculations, summarized here, reveal that in aerosol-based (vapor-precursor) processes, absolute temperature at particle

inception is the most important factor determining ultimate spherule size in both cooling- and heating-environments. This is attributed to the exponential dependence of the (surface-) diffusion-controlled coalescence rate on temperature. In a cooling environment, particle precursor loading also has a pronounced effect on ultimate spherule size, because the high initial temperature is associated with higher rates of Brownian coagulation where the coalescence rates are rapid enough to 'keep pace'. For cooling- (quenching-) rates within the practically attainable range, the magnitude of the quench rate has little effect on ultimate spherule size because, in such an environment, the particles have already experienced peak temperature and, thus, have already reached their maximum size, with further evolution leading just to Brownian aggregation. The situation is different in heating cases, where the spherules are more likely to grow larger by the merger of adjacent spherules as the temperature increases. This will continue until their size will reduce the rate of coalescence compared to that of Brownian-motion-induced collision. Thereafter, large fractal aggregates form with little further alteration of their constituent spherule sizes. In a heating environment, like that encountered on the fuel side of a laminar counterflow diffusion flame (Xing et al., 1996; Chung & Katz, 1985; Gomez & Rosner, 1993), further processing often leads to the ultimate collapse of these aggregates near the bulk material melting temperature, forming much larger isolated particles (Xing et al., 1996; Zachariah & Semerjian, 1989). Results from our modeling studies (Tandon & Rosner, 1999) suggest that lower temperature synthesis can be an effective route to smaller nanoparticles, though precursor loading in a cooling environment must also be limited. Additionally, spherule size may often be economically controlled by invoking other means to change the coalescence rate, for example, introducing 'surface-active' trace additives or dopants (Akhtar et al., 1992).

The extended coalescence–coagulation rate model proposed here, which accounts for enhanced surface diffusivity on nanoparticles, enables us to satisfactorily simulate nanoparticle evolution in non-isothermal aerosol processes involving simultaneous Brownian coagulation. Predictions of absolute spherule sizes, and associated specific surface areas, are found to be in good agreement with available experimental results on pure alumina or pure titania, including our own observations of alumina nanospherule size. Further testing and extensions of the promising, general approach outlined here are in progress. When combined with parallel studies of the joint *pdf* of particle volume and surface area in such environments (Tandon & Rosner, 1999; Rosner & Yu, 1999), it should not only be possible to make improved *Sol Reaction Engineering* (SRE) predictions, but also extract valuable rate parameters from well-defined laboratory experiments on populations of coagulating, restructuring nanoparticles (Xing, 1997).

Acknowledgements

It is a pleasure to acknowledge the financial support of NSF (Yale Grant CTS-9871885) and AFOSR (Yale Grant F49620-97-1-026), and the Yale HTCRE Lab industrial Affiliate, duPont. Helpful discussions with J. Fernandez de la Mora, J.L. Katz, D. Wu, A.V. Filippov, P. Tandon and S. Yu are also gratefully acknowledged.

References

Akhtar M.K., S.E. Pratsinis & S.V.R. Mastrangelo, 1992. J. Am. Ceram. Soc. 75, 3408.
Astier M. & P. Vergnon, 1976. J. Solid State Chem. 19, 67.
Berry R.S., 1997. Microscale Thermophysical Eng. 1, 1.
Bonevich J.E. & L.D. Marks, 1992. J. Mater. Res. 7, 1489.
Broughton J.Q. & G.H. Glimer, 1983. J. Chem. Phys. 79, 5119.
Chase M.W., 1986. 'JANAF Thermochemical Tables', 3rd ed., ACS and AIP.
Chessac P., R. Kofman, R. Garrigos, 1988. Phys. Scr. 38, 164.
Chung S.L. & J.L. Katz, 1985. Combust. Flame 61, 271.
Coblenz W.S., J.M. Dynys, R.M. Cannon & R.L. Coble 1980. Mater. Sci. Res. 13, 141.
Couchman P.R. & W.A. Jesser, 1977. Nature 269, 481.
Flagan R.C. & M.M. Lunden, 1995. Mater. Sci. Eng. A204, 113.
Friedlander S.K., 1977. 'Smoke, Dust and Haze', Wiley, New York.
Gomez A. & D.E. Rosner, 1993. Combust. Sci. Tech. 89, 335.
Helble J.J. & A.F. Sarofim, 1989. J. Colloid Interface Sci. 128, 348.
Huang Y.K., A.A. Menovsky & F.R. de Boer, 1991. Z. Phys. D20, 293.
Ichinose N., Y. Ozaki & S. Kashu, 1992. 'Superfine Particle Technology', Springer-Verlag, London.
Koch W. & S.K. Friedlander, 1990a, J. Colloid Interface Sci. 140, 419.
Koch W. & S.K. Friedlander, 1990b, J. Aerosol Sci. 21, S73.
Kofman R., P. Cheyssac, A. Aouaj, Y. Lereah, G. Deutscher, T. Ben-David, J.M. Penisson & A. Bourret, 1994. Surf. Sci. 303, 231.
Kruis F.E., K.A. Kusters & S.E. Pratsinis, 1993, Aerosol Sci. Tech. 19, 514.

Kusunoki M., K. Yonimitsu, Y. Sasaki & Y. Kubo, 1993, J. Am. Ceram. Soc. 76, 763.
Lai F.S., S.K. Friedlander, J. Pich & G.M. Hidy, 1972. J. Colloid Interface Sci. 39, 395.
Lehtinen K.E.J., R.S. Windeler & S.K. Friedlander, 1996a. J. Aerosol Sci. 27, 883.
Lehtinen K.E.J., R.S. Windeler & S.K. Friedlander, 1996b. J. Colloid Interface Sci. 182, 606.
Lowen H., 1994. Phys. Rep. 237, 249.
Machlin E.S., 1991. An Introduction to Thermodynamics and Kinetics Relevant to Materials Science. Giro Press, Croton-On-Hudson.
Mackrodt W.C., 1992. Phil. Trans. Roy. Soc. Lond. A341, 301.
Matsoukas T. & S.K. Friedlander, 1991. J. Colloid Interface Sci. 146, 495.
Okuyama K., J.-T. Jeung, Y. Kousaka, H.V. Nguyen, J.J. Wu & R.C. Flagan, 1989. Chem. Eng. Sci. 44, 1369.
Oliver P.M., G.W. Watson, E.T. Kelsey & S.C. Parker, 1997. J. Mater. Chem. 7, 563.
Pluis B., D. Frenkel & J.F. van der Veen, 1990. Surf. Sci. 239, 282.
Pratsinis S.E., 1998. Prog. Energy Combust. Sci. 24, 197.
Pratsinis S.E., 1988. J. Colloid Interface Sci. 124, 416.
Pratsinis S.E. & P.T. Spicer, 1998. Chem. Eng. Sci. (in press).
Rosner D.E., 1986. Transport Processes in Chemically Reacting Flow Systems. Butterworths, Boston. Dover ed. (paperback) in press, 1999.
Rosner, D.E. & S. Yu, 1999. 'Monte-Carlo simulation of free-molecule regime Brownian aggregation and simultaneous spheroidization? AIChE J. (submitted May 1999).
Rulison A.J., P.F. Miquel & J.L. Katz, 1996. J. Mater. Res. 11, 3083.
Samsonov G.V., 1982. The Oxide Handbook, IFI/Plenum, New York.
Seebauer E.G. & C.E. Allen, 1995. Prog. Surf. Sci. 49, 265.
Seto T., M. Shimada & K. Okuyama, 1995. Aerosol Sci. Tech. 23, 183.
Somorjai G.A., 1994. Introduction to Surface Chemistry and Catalysis, Wiley, New York.
Tandon P. & D.E. Rosner, 1996. Chem. Eng. Comm. 151, 147.
Tandon P. & D.E. Rosner, 1995. Ind. Eng. Chem. Res. 34, 3265.
Tandon P. & D.E. Rosner, 1999. J. Colloid Interface Sci. 213, 273–286.
Ulrich G.D., 1971. Combust. Sci. Tech. 44, 7.
Ulrich G.D. & N.S. Subramanian, 1977. Combust. Sci. Tech. 17, 119.
Van de Veen J.F., B. Pluis & A.W.D. Van de Gon, 1988. In Vanselow, R. and Howe, R.F., eds. Chemistry and Physics of Solid Surfaces VII. Springer, New York.
Vemury S. & S.E. Pratsinis, 1995. J. Aerosol Sci. 26, 175.
Wu M.K., R.S. Windler, C.K. Steiner, T. Boris, & S.K. Friedlander, 1993. Aerosol Sci. Tech. 19, 527.
Wu M.K. & S.K. Friedlander, 1993. J. Aerosol Sci. 24, 273.
Xing Y., U.O. Koylu & D.E. Rosner, 1996. Combust. Flame 107, 85.
Xing Y., 1997. Synthesis and morphological evolution of metal oxide nanoparticles in flames, Ph.D. Thesis, Yale University.
Xing Y. & D.E. Rosner, 1997. MRS Symp. Proc. 457, 167.
Xing Y., U.O. Koylu & D.E. Rosner, 1999. Appl. Optics 38, 2686.
Xiong Y. & S.E. Pratsinis, 1993. J. Aerosol Sci. 24, 283.
Zachariah M.R. & H.G. Semerjian, 1989. AIChE J. 35, 2003.
Zachariah M.R. & M.J. Carrier, 1994. MRS Symp. Proc. 351, 343.
Zhu W. & S.E. Pratsinis, 1996. In Chow, G.-M. and Gonsalves, K.E., eds. Nanotechnology: Molecular Designed Materials. ACS, Washington.

REPORT DOCUMENTATION PAGE

Form Approved
OMB No. 0704-0188

1. AGENCY USE ONLY (Leave blank)	2. REPORT DATE	3. REPORT TYPE AND DATES COVERED
	March 2000	Reprint

4. TITLE AND SUBTITLE

(U) PARTICLE MORPHOLOGY- AND KNUDSEN TRANSITION-EFFECTS ON THERMOPHORETICALLY DOMINATED TOTAL MASS DEPOSITION RATES FROM "COAGULATION-AGED" AEROSOL POPULATION

5. FUNDING NUMBERS

PE - 61102F
PR - 2308
SA - BS
G-F49620-97-1-0266

6. AUTHOR(S)

Daniel E. Rosner and Y.F.Khalil

7. PERFORMING ORGANIZATION NAME(S) AND ADDRESS(ES)

Yale University
High Temperature Chemical Reaction Engineering Laboratory
Department of Chemical Engineering
PO Box 208286 YS, New Haven, CT 06520-8286 USA

8. PERFORMING ORGANIZATION REPORT NUMBER

9. SPONSORING/MONITORING AGENCY NAME(S) AND ADDRESS(ES)

AFOSR/NA
801 N Randolph St., Rm. 732
Arlington VA 22203-1977

10. SPONSORING/MONITORING AGENCY REPORT NUMBER

11. SUPPLEMENTARY NOTES

J. Aerosol Sci. Vol. 31, No. 3, pp. 273–292, 2000

Printed in Great Britain
0021-8502/00 $ - see front matter

12a. DISTRIBUTION/AVAILABILITY STATEMENT

Approved for public release; distribution is unlimited

12b. DISTRIBUTION CODE

13. ABSTRACT *(Maximum 200 words)*

Abstract Smokes or mists of industrial and environmental interest are typically comprised of particles both large and small compared to the prevailing gas mean-free-path. This fact complicates accurate predictions of, say, *total mass deposition rates* to confining cold walls or immersed cooled objects by the mechanism of particle *thermophoresis* (with Sc ≫ 1) (across laminar- or turbulent-, forced- or natural- convection boundary layers) since particle thermophoretic diffusivities can be sensitive to the prevailing Knudsen number based on individual particle diameter. When taken into account over the entire particle size spectrum, this often reduces the contribution that the largest particles make to the total deposition rate, especially if they are excellent thermal conductors (e.g. unaggregated metals). In the present paper we extend previous results from this group [Rosner.1989, 'Total mass deposition rates from polydispersed aerosols'. *A.I.Ch.E. J.* **34**(1), 164–167; Rosner and Tassopoulos.1989, 'Deposition rates from polydispersed particle populations of arbitrary spread'. *A.I.Ch.E. J.* **35**(9), 1497–1508; Rosner and Khalil, 1997, 'Morphology effects on polydispersed aerosol deposition rates'. *Trans. Amer. Nucl. Soc.* **77** TANSAO 77-1-560, 425–427], to show how total mass deposition rates from a dilute flowing stream of coagulation-aged polydispersed spherical particles in the Knudsen *transition* regime can be conveniently predicted by systematically correcting results more easily calculated for the (hypothetical) *reference* case of 'monodispersed' spheres in the *free-molecule* limit at the same particle mass-loading, ΔT, T_∞, Reynolds-(or Grashof-) number and thermal conductivity ratio: k_p/k_g. For this purpose we carry out "once-and-for-all" quadratures over the Talbot *et al.* (1980) "transition-regime" thermophoretic coefficient function, convoluted with appropriate quasi-self-preserving particle size distribution (PSD-) functions, using recent information on the effective spreads ($\sigma_{g,eff}$) of these near-log-normal PSDs associated with Brownian coagulation in the transition regime (Otto *et al.*, 1994). This leads us to rational, "universal" *deposition rate ratio correlations* of our formally exact quadrature results, expressible in terms only of a prevailing Knudsen number based on *mean* particle size in the population, and the intrinsic thermal conductivity ratio, $\kappa \equiv k_p/k_g$. The availability of these new computational results and dimensionless correlations, remarkably applicable to both laminar and turbulent boundary layer particle transport and natural or forced-convection, will dramatically simplify and accelerate such multi-size particle thermophoretically dominated aerosol deposition rate calculations in a wide variety of engineering applications.

14. SUBJECT TERMS

Laser-induced incandescence. soot morphology , aggregated particles, particle mass transport thermophoresis, Brownian diffusion, particle sampling, nano-particle formation/restructuring in flames, deposition rate theory

15. NUMBER OF PAGES

20

16. PRICE CODE

17. SECURITY CLASSIFICATION OF REPORT	18. SECURITY CLASSIFICATION OF THIS PAGE	19. SECURITY CLASSIFICATION OF ABSTRACT	20. LIMITATION OF ABSTRACT
Unclassified	Unclassified	Unclassified	UL

Pergamon

www.elsevier.com/locate/jaerosci

PII: S0021-8502(99)00054-3

J. Aerosol Sci. Vol. 31, No. 3, pp. 273–292, 2000

Printed in Great Britain
0021-8502/00 $- see front matter

PARTICLE MORPHOLOGY- AND KNUDSEN TRANSITION-EFFECTS ON THERMOPHORETICALLY DOMINATED TOTAL MASS DEPOSITION RATES FROM "COAGULATION-AGED" AEROSOL POPULATION*

Daniel E. Rosner† and Yehia F. Khalil‡

Yale University, Department of Chemical Engineering, High Temperature Chemical Reaction Engineering Laboratory, New Haven, CT 06520-8286, U.S.A.

Abstract—Smokes or mists of industrial and environmental interest are typically comprised of particles both large and small compared to the prevailing gas mean-free-path. This fact complicates accurate predictions of, say, *total mass deposition rates* to confining cold walls or immersed cooled objects by the mechanism of particle *thermophoresis* (with $Sc \gg 1$) (across laminar—or turbulent-, forced—or natural—convection boundary layers) since particle thermophoretic diffusivities can be sensitive to the prevailing Knudsen number based on individual particle diameter. When taken into account over the entire particle size spectrum, this often reduces the contribution that the largest particles make to the total deposition rate, especially if they are excellent thermal conductors (e.g. unaggregated metals). In the present paper we extend previous results from this group [Rosner,1989, 'Total mass deposition rates from polydispersed aerosols', *A.I.Ch.E. J.* **34**(1), 164–167; Rosner and Tassopoulos,1989, 'Deposition rates from polydispersed particle populations of arbitrary spread', *A.I.Ch.E. J* **35**(9), 1497–1508; Rosner and Khalil, 1997, 'Morphology effects on polydispersed aerosol deposition rates', *Trans. Amer. Nucl. Soc.* 77 TANSAO 77-1-560, 425–427], to show how total mass deposition rates from a dilute flowing stream of coagulation-aged polydispersed spherical particles in the Knudsen *transition* regime can be conveniently predicted by systematically correcting results more easily calculated for the (hypothetical) *reference* case of 'monodispersed' spheres in the *free-molecule* limit at the same particle mass-loading, $\Delta T/T_w$, Reynolds-(or Grashof-) number and thermal conductivity ratio: k_p/k_g. For this purpose we carry out "once-and-for-all" quadratures over the Talbot *et al.* (1980) "transition-regime" thermophoretic coefficient function, convoluted with appropriate quasi-self-preserving particle size distribution (PSD-) functions, using recent information on the effective spreads ($\sigma_{g,eff}$) of these near-log-normal PSDs associated with Brownian coagulation in the transition regime (Otto *et al.*, 1994). This leads us to rational, "universal" *deposition rate ratio correlations* of our formally exact quadrature results, expressible in terms only of a prevailing Knudsen number based on *mean* particle size in the population, and the intrinsic thermal conductivity ratio: $\kappa \equiv k_p/k_g$. The availability of these new computational results and dimensionless correlations, remarkably applicable to both laminar and turbulent boundary layer particle transport and natural or forced-convection, will dramatically simplify and accelerate such multi-size particle thermophoretically dominated aerosol deposition rate calculations in a wide variety of engineering applications. While a comprehensive theory for *aggregate* thermophoresis is not yet available (see, e.g. Rosner *et al.*, 1991), provisional results are also included here for the morphologically opposite limiting case of aggregated particles (fractal morphology; not "fully dense" spheres). Our results indicate that the thermophoretic deposition rates of aggregates of conductive materials will remain high at *all* Knudsen numbers due to the poor *effective thermal conductivity* of such aggregates.

NOMENCLATURE

B_T	dimensionless thermophoretic "suction" Peclet number; equation (19)
C_{slip}	Cunningham–Millikan slip flow correction factor to Stokes drag; equation 3
d_g	particle diameter corresponding to r_g
d_f	spherule diameter ("primary" particles in aggregate)
D_p	Brownian diffusion coefficient for particle of volume v
D_f	fractal exponent ("dimension") describing morphology of aggregate population
$f(x)$	function defined by equation (10)

* Supported by AFOSR (Grant 97-1-0266), NASA (Grant NAG 3-1951), AGARD/NATO (Grant p-125) and the Yale-HTCRE Lab Industrial Affilite: duPont.
† Author to whom correspondence should be addressed. E-mail: daniel.rosner@[redacted]yale.edu
‡ Research Affiliate, ChE Department.

g	gravitational acceleration
k_{eff}	effective thermal conductivity
k_p	thermal conductivity of the particle substance
k_g	thermal conductivity of the background (carrier) gas
k_{gyr}	prefactor in fractal relation based on *gyration* radius of aggregate(s)
k_B	Boltzmann constant
Kn_p	Knudsen number based on prevailing gas mean-free path and particle diameter
Kn_1	Knudsen number based on prevailing gas mean-free path and spherule diameter
L	reference length (for Re, Nu_m, etc.)
l_g	gaseous *molecule mean free path*
m	slope defined by equation (18)
$\dot{m}$	particle mass deposition rate to cold surface of interest
m_p	mass of particle of volume v
M_k	kth moment of PSD $n(v, \ldots) = \mathrm{d}N_p/\mathrm{d}v$
n	size distribution function $\mathrm{d}N_p/\mathrm{d}v$
N_p	total particle number density ($= M_0$)
Nu_m	mass transfer Nusselt (Sherwood) number (see, e.g. Rosner (1990))
Pr	Prandtl number for carrier gas, $\nu/(k/(\rho c_p))$
Re	Reynolds number UL/ν, based reference velocity U
$\mathscr{R}$	deposition rate ratio calculated via equation (4)
Sc	particle Schmidt number, $(\mu/\rho)_{gas}/D$p
St_m	mass transfer Stanton number, $\mathrm{Nu}_m/(\mathrm{Re}\,\mathrm{Sc})$ (Rosner, 1986)
t_p	particle "stopping time" in the prevailing carrier gas (see, e.g. Friedlander, 1977)
T	absolute temperature
U	mean velocity of carrier gas (forced convection)
u	particle volume (dummy variable)
v	volume of condensed material in spherical particle or aggregate
v_g	geometric-mean particle volume in log-normal PSD $n(v, \ldots)$
$\bar{v}$	mean particle volume, ϕ_p/N_p, of local aerosol
w_j	weight factors in the Gauss–Hermite quadrature relation: equation (11)
x	integration variable in Gauss–Hermite quadrature, equation (8)

Greek letters

$\alpha_T D$	particle thermophoretic diffusivity: (particle drift velocity)/((-**grad** T)/T)
α_h	thermal diffusivity of carrier gas mixture, $k/(\rho c_p)$
α_{mom}	gas/surface momentum accommodation coefficient
α	dimensionless thermophoretic diffusivity, $\alpha_T D_p/\nu$ (see, e.g. Fig. 2)
$\beta(u, v)$	coagulation rate constant in "mass-action" law (used to calculate coagulation time)
δ	gaseous boundary layer thickness
ε	$1/(10 \cdot \mathrm{Kn}_c)$; small parameter in equation (14)
η	dimensionless particle volume, $v/\bar{v}$
ϕ_p	particle volume fraction ($= M_1$); $\bar{v} N_p$
κ	thermal conductivity ratio: k_p/k_g
ρ_p	intrinsic density of a particle (m_p/v_p)
μ_k	dimensionless kth moment of dimensionless PSD: $\psi(\eta)$ ($\mu_0 = 1$, $\mu_1 = 1$)
μ_{gas}	dynamic Newtonian viscosity of the carrier gas
ψ	dimensionless PSD, $\bar{v} \cdot n(v, \ldots)/N_p$
σ_g	geometric standard deviation of the log-normal PSD $n(v, \ldots,)$ (see, e.g. Rosner and Tassopoulos, 1989)
ν	momentum diffusivity ("kinematic viscosity") of the carrier gas, $(\mu/\rho)_{gas}$

Subscripts

c	continuum limit ($\mathrm{Kn}_p \ll 1$)
coag	coagulation
coalesc	coalescence
eff	effective value
e	outer edge of the boundary layer
fm	free-molecule limit ($\mathrm{Kn}_p \gg 1$)
g	pertaining to log-normal PSD (geometric)
gas	pertaining to the carrier gas
gyr	gyration
h	heat transfer (thermal BL)
infl	inflection point
k	pertaining to moment k, where k need *not* be an integer, nor positive
m	mass transfer (particle mass transfer BL)
max	maximum value
p	particle(s)
ref	reference value
T	thermophoretic
$\bar{v}$	pertaining to the length $(6\bar{v}/\pi)^{1/3}$
w	evaluated at the wall (gas/solid interface)
1	pertaining to the "primary" spherules
∞	"far" from the deposition surface (in multiples of δ_T)

Other

$(\bar{\ })$	mean value (e.g. $\bar{v} = \phi_p/N_p$, $\bar{d} = (6\bar{v}/\pi)^{1/3}$)
$(\ )''$	per unit area
Δ	change in (operator); $\Delta T = T_c - T_w$
$(\ )$	argument of a function

Abbreviations/Acronyms

BL	boundary layer
c	continuum limit ($\mathrm{Kn}_p \ll 1$)
coag	pertaining to (Brownian) coagulation
C–C	cluster–cluster (aggregate–aggregate)
fm	free-molecule limit ($\mathrm{Kn}_p \gg 1$)
GHQ	Gauss–Hermite quadrature (Section 3.5)
log	logarithm (to base 10)
LBL	laminar boundary layer
mfp	gaseous *molecule mean free path*
TBL	turbulent boundary layer
PSD	particle size (volume) distribution

1. INTRODUCTION, BACKGROUND, OBJECTIVES

The fact that condensation aerosols ("smokes") of industrial interest are not comprised of dense, isolated spherical particles of only one size inevitably complicates the prediction of, say, *wall deposition rates*, but must, of course, be accurately taken into account. In general, we have been seeking rational yet convenient methods to take into account the systematic effects on *total mass deposition rates* of: aerosol "polydispersity", rarefaction (Knudsen transition behavior), particle properties (e.g. thermal conductivity effects on thermophoretic deposition), and aerosol particle morphology (aggregates vs dense spheres).

In the present paper we extend previous results from this group (Rosner, 1989,1998a, b; Rosner and Tassopoulos, 1989; Rosner and Khalil, 1997) to show how *thermophoretically dominated* total mass deposition rates from a dilute flowing stream of coagulation-aged polydispersed spherical particles in the Knudsen *transition* regime can be conveniently predicted by systematically correcting results more easily calculated for the (hypothetical) *reference* case of "monodispersed" spheres in the *free-molecule* limit at the same particle mass-loading, $\Delta T/T_w$, Reynolds- or Grashof-number and thermal conductivity ratio: k_p/k_g. For this purpose we carry out "once-and-for-all" quadratures over the Talbot *et.al.* (1980) "transition-regime" thermophoretic coefficient function, convoluted with appropriate quasi-self-preserving particle size distribution (PSD-) functions, using recent information on the effective spreads ($\sigma_{g,\mathrm{eff}}$) of these near-log-normal PSDs (Wu and Friedlander 1993; Tandon and Rosner, 1999) associated with Brownian coagulation in the transition regime (Otto *et al.*, 1994). This will be shown to lead to rational, "universal" *deposition rate ratio correlations* of our formally exact quadrature results (Figs 4, 6), expressible in terms only of a prevailing Knudsen number based on *mean* particle size in the population, and the intrinsic thermal conductivity ratio: k_p/k_g. The availability of these new computational results and dimensionless correlations (equations (17) and (18)), applicable to both laminar and turbulent boundary layer transport in forced- or natural-convection systems, is shown to dramatically simplify and accelerate such multi-size particle thermophoretically dominated aerosol deposition rate calculations in a wide variety of engineering applications. Provisional results are also included for aggregated particles (fractal morphology; not "fully dense"). For this latter purpose we make use of recent information on: (a) the size and morphology dependence of individual particle transport properties (Garcia-Ybarra and Rosner, 1988; Rosner *et al.*, 1991, 1992; Rosner and Tandon, 1995); (b) the spreads (σ_g) of log-normal *aggregate* particle size distribution (PSD-) functions due to Brownian coagulation in the Knudsen and continuum regimes and (c) the fractal properties (exponent D_f) of the constituent multi-spherule aggregates (Megaridis and Dobbins, 1990; Koylu *et al.*, 1995; Neimark *et al.* 1996). While our specific illustrations in this paper (Section 5) deal with deposition mechanism of *thermophoresis*, the same strategy can be successfully adopted/implemented for particle deposition by the mechanisms of convective-diffusion, gravitational sedimentation and "eddy-impaction", for laminar or turbulent flow with

particles of negligible mass fraction (Park and Rosner, 1989a, b) and not all small enough to be in the free-molecule ($Kn_p \gg 1$) regime at the prevailing pressure level.

2. PRINCIPAL ASSUMPTIONS; APPROACH

In keeping with our goal of obtaining generally applicable deposition rate results for *thermophoresis* from coagulation-aged polydispersed particle populations in terms of a small number of governing dimensionless groups, we explicitly make the following fundamental assumptions and idealizations:

A1: The local mainstream aerosol population is Brownian-"coagulation-aged" and approximately "log-normal" in terms of particle size (cf. Fig. 1).

A2: Particle volume and mass-fractal "dimension" adequately characterize the particle "state" (with $D_f = 3$ for dense coalesced spheres and $D_f = 1.7$ for "Cluster–Cluster" aggregates (Sections 3.8, 4.3).

A3: The dominant particle deposition mechanism is *thermophoretic transport* to cooled solid surfaces (either immersed in or confining the hot, aerosol-containing gas).

A4: All particles in the population have the same intrinsic thermal conductivity and mass density.

A5: The suspended particle *mass* fraction is low (< 0.01), corresponding to even smaller *volume* fractions (typically of order: 0.1–10 ppm).

A6: Particles of different sizes do not appreciably interact *during* the transport process across laminar or turbulent BLs leading to deposition.[§]

A7: Arriving particles are permanently captured by the cold wall with an effective capture fraction of unity.

We postpone a brief but critical examination of the limits of validity of these assumptions to Section 6, which includes explicit quantitative criteria, and suggestions or pertinent references for dealing with more complex stuations (where one or more of these idealizations may require generalization).

3. FORMULATION OF DEPOSITION RATE RATIO $\mathscr{R}\{Kn_{\bar{v}}, k_p/k_g\}$ FOR $D_f = 3$

3.1. *Dependence of St_m on thermophoretic coefficient; LBL or TBL when $Sc \gg 1$, modest temperature contrast*

Mainly in the last two decades, there have been numerous theoretical studies of the laws governing thermophoretically dominated particle mass transport from flowing gases (see, e.g. Goren, 1977; Rosner and Fernandez de la Mora, 1982; Gokoglu and Rosner, 1984; Rosner and Park, 1986; Batchelor and Shen, 1985; Epstein *et al.*, 1985; and, most recently, Garcia-Ybarra and Castillo, 1997). Most of the above deal with $Sc \gg 1$ laminar forced-convection boundary layers (LBLs), but also included are *natural* convection, and law-of-the-wall *turbulent* boundary layers (TBLs). There have been fewer relevant experimental studies (Rosner and Kim, 1984; Eisner and Rosner, 1985; Makel and Kennedy, 1991; Konstandopoulos and Rosner, 1995), but it is clear from *all* of the above studies that there is an important domain of temperature "contrasts" (say, as measured by the departure of the absolute temperature ratio T_w/T_∞ from unity) in which: (a) thermophoresis is the dominant particle mass transfer mechanism, and (b) the relevant mass transfer coefficient St_m is *nearly linear* in the dimensionless thermophoretic coefficient $\alpha \equiv \alpha_T D_p/\nu$ discussed below

[§] Interestingly enough, this condition need not be imposed for the case of $D_f = 1.7$ (Section 3.8) since in that case BL coagulation would have little influence on the effective thermophoretic diffusivity and the associated mass transfer coefficient (see Fig. 6 and Park and Rosner, 1989).

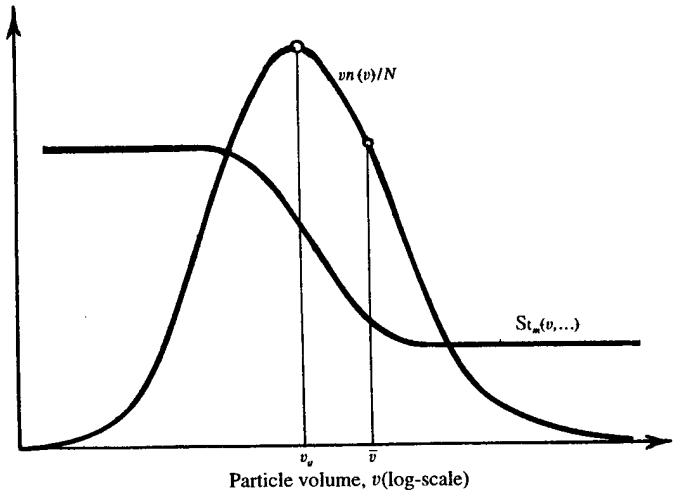

Fig. 1. Schematic showing both the particle size dependence of the operative *mass transfer coefficient* St_m and the local mainstream *volume distribution function* vs. log (particle volume) (cf. Rosner, 1989; Rosner and Tassopoulos, 1989).

(Section 3.2). From the usual definitions of convective[¶] mass transfer coefficient (see, e.g. Rosner, and continuous particle size distribution function, $n(v)$, in the vicinity of the collector 1986) we can express the local total mass deposition rate per unit area of cooled surface as a quadrature (see, e.g. Rosner, 1989):

$$\dot{m}'' = \int_0^\infty U\,St_m\{\alpha, Re, Pr, \ldots\} \cdot \rho_p \cdot v \cdot n\{v, \ldots\}\,dv, \tag{1}$$

where, in accord with A4, all non-aggregated particles in the distribution will be assumed to have the same intrinsic mass density, ρ_p, and thermal conductivity. In what follows we will combine the above mentioned linearity of $St_m\{\alpha, Re, Pr, \ldots\}$ with respect to α with the theory of the thermophoretic coefficient for dense spherical aerosol particles (Section 3.2) to carry out, once-and-for-all, a dimensionless form of this integral. In the case of *aggregated* particles we provide in Section 3.8 a plausible generalization to anticipate the corresponding total mass deposition rate behavior for $D_f = 1.7$.

3.2. *Dependence of thermophoretic diffusivity $\alpha_T D_p$ on Kn and k_p/k_g*

Talbot (1980) reviewed the isolated solid sphere thermophoretic literature as of 1980 and was able to recommend a semi-theoretical/empirical formula for the dimensionless thermophoretic coefficient, $\alpha \equiv \alpha_T D_p/\nu$, consistent with available theoretical results in the two asymptotic limits (near-continuum, and near free-molecule) as well as available experimental data on particles covering a wide range of intrinsic thermal conductivities. He recommended, in our notation

$$\frac{\alpha_T D_p}{\nu} \equiv \alpha = \frac{2.34[\kappa^{-1} + 4.36\,Kn_p]\cdot C_{slip}\{Kn_p\}}{[1 + 2\kappa^{-1} + 8.72\,Kn_p]\cdot[1 + 6.84\,Kn_p]}, \tag{2}$$

[¶] We are here explicitly considering a *forced*-convection environment where there is an obvious physical choice of reference velocity, U. However, our present formulation/results apply equally well to *natural* (i.e. bouyancy-induced-) convection aerosol systems, in which case U_{ref} can be regarded to be: $\{g\cdot(\Delta T/T)L_{ref}\}^{1/2}$ (see, e.g. Rosner, 1986).

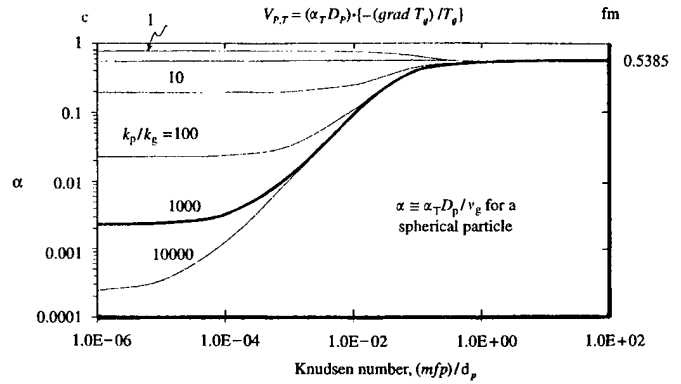

Fig. 2. Dependence of dimensionless thermophoretic diffusivity, $\alpha = \alpha_T D_p/\nu$ for a solid sphere on Knudsen number and thermal conductivity ratio $\kappa = k_p/k_g$, based on the equation of Talbot (1980) for $D_f = 3$.

where the coefficients appearing in this relation have been assigned numerical values pertinent to high effective gas/solid accommodation coefficients (see, e.g. Rosner and Papadopoulos, 1996), and C_{slip} is the familiar Cunningham–Millikan–Stokes "slip-flow" drag correction factor

$$C_{slip}\{\mathrm{Kn_p}\} = 1 + 2\mathrm{Kn_p}\cdot\{A_1 + A_2\ \exp\{-A_3/\mathrm{Kn_p}\}\}. \tag{3}$$

where we have used: $A_1 = 1.257$, $A_2 = 0.4$, $A_3 = 0.55$. Figure 2 shows a log–log graph of this important "α"-function, revealing a fm-limit value of 0.567[‖] and the decreased thermophoretic drift of highly conductive particles as one enters the continuum regime (low Knudsen numbers based on individual particle diameter). As detailed below, this "Talbot function" is incorporated into our present dimensionless formulation of the total mass deposition rates from populations of uniformly dense spherical particles distributed with respect to size, but not thermal conductivity or density. The remarkable behavior for thermal conductivity ratios in the range: $1 < k_p/k_g < 2.12$ will prove to be important in understanding the behavior of *aggregated* particles, because of their low "effective" thermal conductivity (see below).

Because of their technological importance it would be valuable to have a reliable Talbot function for large 'fractal' *aggregates* (e.g. $D_f = 1.7$ rather than 3), as commonly observed in sooting combustors (see, e.g. Koylu *et al.*, 1995). While no accepted theory is yet available, we have made a plausible tentative estimate of this "modified" function (Rosner, 1998) based on the "effective sphere" reasoning outlined in Section 3.8 below.

3.3. *Quadrature relation for* $\mathscr{R}\{Kn_{\bar{v}}, k_p/k_g, \ldots\}$

Since we will be dealing with deposition from "coagulation-aged" populations (Assumption 1) it will be convenient to use appropriately rescaled dimensionless variables for the size distribution function, $\psi \equiv \bar{v}n\{v, \ldots\}/N_p$, and particle volume $\eta \equiv v/\bar{v}$. In our expression for the deposition rate ratio: $\mathscr{R} \equiv \dot{m}/\dot{m}_{ref}$, we also choose $\dot{m}_{ref}$ to be the thermophoretic mass deposition rate under the prevailing conditions but assuming all particles had the *mean* volume, and with the thermophoretic coefficient (Section 3.2) formally evaluated in the free-molecule (fm-) limit. If all particles have the same density and intrinsic thermal conductivity then the above mentioned *deposition rate ratio* can be conveniently expressed

[‖] Compare this to the (5.3% lower) Waldmann (exact) *fm* limit value: $(3/4)\cdot[1 + (\pi\alpha/8)]^{-1} = 0.53852$ for $\alpha_{mom} = 1$ (cf. Garcia-Ybarra and Rosner (1989).

in the compact quadrature form

$$\mathscr{R}\{\mathrm{Kn}, k_p/k_g\} = \int_0^\infty (\alpha/\alpha_{fm})\cdot\eta\psi\{\eta;\mathrm{Kn}\}\,d\eta, \tag{4}$$

where the Knudsen number (based on mean particle size) enters both *via* the evaluation of the normalized thermophoretic coefficient α/α_{fm} as a function of particle size, η, and *via* the spread of the "quasi-self-preserving" particle size distribution function $\psi(\eta)$ (see, e.g. Otto *et al.*, 1994).

In what follows (Sections 3.4 and 3.5) we exploit the fact that numerically generated particle volume distribution functions $\eta\psi\{\eta\}$ have been found to be well-represented by log-normal functions (i.e. they are nearly Gaussian in terms of log (volume)). This allows us to relate the median volume to the mean volume *via*: equation (9) of Rosner and Tassopoulos (1989)), i.e.

$$\bar{v} = v_g \exp\{(\tfrac{1}{2})\ln^2\sigma_g\}, \tag{5}$$

where σ_g is the effective *spread parameter* discussed below. It also facilitates the numerical integrations themselves (Section 3.5), since efficient Gauss quadrature formulae are available for infinite domains and integrands dominated by a function of the form: $\exp(-x^2)$ (Abramowitz and Stegun, 1964).

3.4. *Log-normal representation of coagulation-aged aerosol populations; spreads in the Knudsen transition regime*

Well before the onset of appreciable gravitational sedimentation contributions to the coagulation rate and deposition rate, binary encounters due to isotropic *particle Brownian motion* will dominate the population dynamics in large, "well-mixed" volumes (Friedlander, 1977; Williams and Loyalka, 1991). For the two limiting cases (free-molecule and continuum-regime Brownian motion) log-normal representations of the corresponding self-preserving function $\eta\psi\{\eta\}$ are comparatively well known for the $D_f = 3$ case, and now also available for the important case of cluster–cluster fractal aggregates with $D_f = 1.7$ (see, e.g. Wu and Friedlander, 1993; Tandon and Rosner, 1999). Recently, Otto *et al.* (1994) have numerically calculated the shapes of aerosol populations in the Knudsen transition regime and shown that these are also near-log-normal but with a spread which is non-monotonic in Knudsen number (based on mean size). Assembling these results leads us to introduce into equation (4) the log-normal distribution function

$$\eta\psi(\eta) = \frac{1}{(2\pi)^{1/2}\ln\sigma_g}\exp\left\{-\frac{\ln^2(\eta/\eta_g)}{2\ln^2\sigma_g}\right\} \tag{6}$$

with $\eta_g = v_g/\bar{v}$, but with the spread parameters shown in Fig. 3 over the entire Knudsen number range. Here we have modified Otto *et al.* asymptotic spreads (to give better estimates of fractional positive moments of the PSD) but adopted their transition behavior *shape* (and converted from their $\mathrm{Kn_g}$ to our $\mathrm{Kn}_{\bar{v}}$).

3.5. *Gauss–Hermite quadrature (GHQ) for numerical results*

In view of equations (1) of each of the three sections above, the quantity of interest can be expressed in the "canonical" form

$$\mathscr{R}\{\mathrm{Kn}_{\bar{v}}, k_p/k_g\} = (\eta_g/\pi^{1/2})\cdot\int_{-\infty}^{\infty} f(x)\cdot\exp\{-x^2\}\,dx, \tag{7}$$

where

$$x \equiv [\ln(\eta/\eta_g)]/(2^{1/2}\ln\sigma_g), \tag{8}$$

$$\eta_g \equiv \exp(-\tfrac{1}{2}\ln^2\sigma_g), \tag{9}$$

and

$$f(x) \equiv \exp\{2^{1/2}(\ln\sigma_g)\cdot x\}\cdot(\alpha/\alpha_{fm}), \tag{10}$$

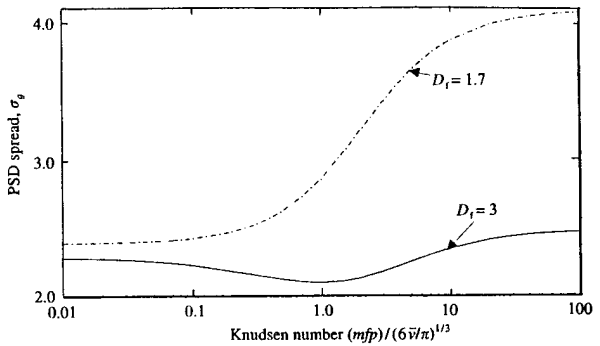

Fig. 3. Assumed Knudsen number dependence of the effective *spreads* of quasi-self-preserving particle populations ($D_f = 3$ results based, in part, on the results of Otto *et al.* (1994); $D_f = 1.7$ results are provisional (Section 3.8 and Vemury and Pratsinis, 1995).

where (α/α_{fm}) is evaluated at the individual particle Knudsen number: $\mathrm{Kn}_{\bar{v}} \cdot \eta^{-1/3}$.

Accordingly, the integral in equation (7) can be efficiently expressed as a weighted sum (Gauss–Hermite quadrature)

$$\int_{-\infty}^{\infty} f(x)\exp\{-x^2\}\,dx = \sum_{j=1}^{\pm n} w_j f\{x_j\}, \tag{11}$$

where the associated *weight factors* w_j and *abscissae* x_j are tabulated in Abramowitz and Stegun (1964). In all cases, at least $n = 10$ integration formulae (corresponding to 20 quadrature points) were used, and it was verified that our results (to three significant figures) were unaltered by this choice.

3.6. *Asymptotic $\mathscr{R}$-results for $D_f = 3$, near-continuum and free-molecule regimes*

Since the function (α/α_{fm}) posesses horizontal asymptotes (see Fig. 2 for the non-normalized Talbot function for $D_f = 3$) in both extremes of Knudsen number, it is useful and straightforward to identify the associated asymptotes for the quantity of interest: $\mathscr{R}(\mathrm{Kn}_{\bar{v}}, k_p/k_g)$. In the free-molecule limit we find

$$\mathscr{R}\{\infty, k_p/k_g\} \equiv \mathscr{R}_{fm} = \mu_1 = 1 \quad \text{for all } k_p/k_g, \tag{12}$$

whereas, in the continuum limit we find

$$\mathscr{R}\{0, k_p/k_g\} \equiv \mathscr{R}_c = (\alpha_c/\alpha_{fm})\cdot\mu_1 = 2.06/[1 + (1/2)(k_p/k_g)]. \tag{13}$$

Indeed, a normalized version of the quantity of interest, viz $(\log\mathscr{R} - \log\mathscr{R}_c)/(\log\mathscr{R}_{fm} - \log\mathscr{R}_c)$ will prove useful in developing a compact correlation of our numerical results (Section 3.7). It would also be useful to have an accurate method to calculate $\mathscr{R}$ when it is only slightly smaller than the free-molecule limit value: unity (see, e.g. Section 5.2.2), i.e. a near-free molecule expansion for $\mathscr{R}$ in powers of the small parameter $\varepsilon \equiv (10\,\mathrm{Kn}_{\bar{r}})^{-1}$ with coefficients that depend on k_p/k_g and moments of the free-molecule near-log-normal PSD. By expanding (α/α_{fm}) in this manner and using equation (4) we find for the first three non-unity terms

$$\mathscr{R} = [1 - \varepsilon + 4.76[1 + (0.556/\kappa)]\cdot\mu_{4/3}\varepsilon^2 - [17.8 + (5.66/\kappa) + (6.06/\kappa^2)]\cdot\mu_{5/3}\varepsilon^3 + \cdots, \tag{14}$$

where the indicated moment-values can be estimated from the log-normal result

$$\mu_k = \exp\{(\tfrac{1}{2})k\cdot(k-1)\cdot\ln^2\sigma_{g,fm}\} \quad \text{with } \sigma_{g,fm} = 2.4. \tag{15}$$

Unfortunately, the rate of convergence of this series is so slow that it is unlikely to be very useful except for very large values of the indicated Knudsen number. Interestingly enough, even the leading non-unity term is *independent* of the thermal conductivity ratio: $\kappa \equiv k_p/k_g$.

3.7. *Correlation procedure for arbitrary Kn, k_p/k_g; $D_f = 3$*

For routine engineering calculations it would be desirable to summarize the results of our formally numerically "exact" quadratures (Sections 3.3 and 4.1) in the form of easily used, acceptably accurate formulae not limited to very large, or very small Knudsen numbers. These were obtained as follows. Based on our numerical GHQ results for $\mathscr{R}\{\mathrm{Kn};\kappa\}$ it was immediately clear that this function has a "tanh" character, and this is, indeed, a convenient function to work with. By forming $[\log\mathscr{R}\log\mathscr{R}_c)/(-\log\mathscr{R}_c)$ we accomplish "normalization" on the log(Kn) abscissa (using logs to the base 10). It remained to (a) enforce the proper location of the inflection points (i.e. the values of log(Kn) where $\mathscr{R} = (\mathscr{R}_{fm}\cdot\mathscr{R}_c)^{1/2}$ and, (b) ensure that each curve (i.e. for each log(κ)) has the proper slope, $d\log\mathscr{R}/d\log\mathrm{Kn}$, at this inflection point.

This was accomplished with the help of two graphs (crossplots). The first was the locus of numerically obtained inflection point locations, which fortunately agreed well with the simple fit:

$$\log(\mathrm{Kn})_{infl} = -0.9 - (\tfrac{1}{2})\cdot\log(\kappa) \quad \text{at } \mathscr{R} = (\mathscr{R}_{fm}\cdot\mathscr{R}_c)^{1/2}. \tag{16}$$

The second was a plot of the numerical slope: $d\log\mathscr{R}/d\log\mathrm{Kn}_{\bar{v}}$ (linear scale) *at* the inflection point vs log(κ). Since this slope nearly vanishes at $\kappa = 2.12$ (where $\mathscr{R}_c$ is also unity), a graph using $\log(\kappa/2.12)$ as the abscissa was first prepared. Fitting this graph, it was found that for $\kappa > 2.12$ the slope at the inflection point can be adequately described** by the equation

$$\left(\frac{d\log\mathscr{R}}{d\log_{10}\mathrm{Kn}_{\bar{v}}}\right)_{infl} \approx \left(\frac{9}{8}\right)\cdot\left\{1 + \left[(0.365)\cdot\log_{10}\left(\frac{\kappa}{2.12}\right)\right]^{-8}\right\}^{-1/8}. \tag{17}$$

Combining these relations led to our suggested tanh-form for estimating $\mathscr{R}(\mathrm{Kn}_{\bar{v}};\kappa)$ when $D_f = 3$:

$$\frac{\log_{10}(\mathscr{R}/\mathscr{R}_c)}{\log_{10}(1/\mathscr{R}_c)} \approx \frac{1}{2}\{1 + \tanh[m\{\kappa\}\cdot\log_{10}(8.19\kappa^{1/2}\cdot\mathrm{Kn}_{\bar{v}})]\}, \tag{18}$$

where $m\{\kappa\}$ is given by the product of equation (17) and $\{(\tfrac{1}{2})\cdot\log(1/\mathscr{R}_c)\}^{-1}$.

As will be illustrated in Section 5, equations (18) and (17) make it easy to calculate total mass deposition rates for polydispersed aerosols with any intrinsic thermal conductivity k_p. Of course, if increased accuracy is required, or if the PSD is a "distorted" log-normal, it is straightforward, and not very computationally demanding, to revert to the underlying quadrature formulation, or to propose a somewhat more complicated functional form for the "curve-fit" with "optimized" coefficients.

3.8. *Provisional formulation of the aggregate ($D_f = 1.7$) case*

Even in combustion environments, most condensing materials are not able to restructure fast enough (see, e.g. Helble and Sarofim, 1989; Koch and Friedlander, 1990; Xing, *et al.*, 1997, 1999) to prevent the formation of tenuous "fractal-like" multispherule aggregates (see, e.g. Koylu *et al.*, 1995; Neimark *et al.*, 1996), so that the laws of particle transport must take

** This choice deliberately overcorrects the local slope somewhat to reduce overall rms deviations.

into account this morphological "fact of life". The consequences for the asymptotic spreads (with respect to aggregate mass or total spherule volume) of approximately log-normal coagulation-aged populations have recently been estimated using Monte-Carlo simulation methods for both the continuum limit (Tandon and Rosner, 1999) and the so-called "free-molecule" limit (Wu and Friedlander, 1993). If all particles in the population are assumed to have a common fractal exponent, D_f, and both the mobility diameter and collision diameter are assumed to scale with total aggregate volume as $(v)^{1/D_f}$, the corresponding spread results are also collected in Fig. 3, with $D_f = 3$ corresponding to the previously well-studied case of uniformly dense spheres. The systematic continuum-regime "narrowing" of the PSD-shape-preserving population (reduced σ_g for $D_f < 3$) is taken into account in the calculations of deposition rate correction factors reported below (Fig. 6). In the absence of population spread information to the contrary, the (non-monotonic) nature of the Knudsen transition between these above mentioned asymptotes was taken to be the same as for the $D_f = 3$ case. As to our provisional estimation of the *aggregate thermophoretic diffusivity*, we imagine that an aggregate behaves like a homogeneous sphere with an effective mobility diameter about equal to the gyration diameter (consistent with earlier estimates of the Brownian collision rate constant), and with an *effective thermal conductivity* equal to that expected for the "granular medium" (of spherules) existing at the gyration radius (for details, see Tandon and Rosner, 1995; Rosner, 1998a). This introduces one new parameter which must be specified besides the aggregate fractal dimension $D_f = 1.7$ (and corresponding pre-factor, $k_{gyr} = 2.4$; Koylu *et al.*, 1995); viz., Kn_1, the Knudsen number based on *spherule* diameter.[††] Accordingly, Fig. 6 (discussed below) will be constructed for the choice: $Kn_1 = 0.3$, representative of carbonaceous soot in a high pressure (ca. 50 atm.) combustor.

4. NUMERICAL RESULTS/DISCUSSION FOR $\mathscr{R}\{Kn_{\bar{v}}, k_p/k_g\}$

4.1. *Results for* $D_f = 3$: $\mathscr{R}\{Kn_{\bar{v}}; k_p/k_g\}$

In Fig. 4 we plot (using log–log coordinates) our GHQ-computed $\mathscr{R}$-values (solid contours) over the important range of intrinsic thermal conductivity ratios up to 10,000. (On the same scale we show (dashed) the corresponding $\mathscr{R}$-results formally computed from our recommended correlation formula (equations (17) and (18); this comparison is briefly discussed in Section 4.2). We illustrate in Section 5.2.1 below how such $\mathscr{R}$-results can be used to predict thermophoretically dominated deposition rates in engineering devices (e.g. those operating at very at high pressures), provided the conditions outlined in Section 2 are satisfied (see, also, the critical discussion in Section 6, along with possible extensions). Remarkably, these results apply to either laminar or turbulent boundary layer situations, and for either "forced"- or "natural"-convection systems. Moreover, the strategy and procedure we have used here to generate these deposition rate ratio results for the $D_f = 3$ case (uniformly dense particles) carry over to our plausible quantitative treatment of the important $D_f = 1.7$ case (aggregated "soot"), as demonstrated in Section 4.3 below.

4.2. *Success of proposed correlation*

The convenient correlation formulae developed/presented in Section 3.7, which were used to generate the (dashed) contours shown in Fig. 4, will be adequate for many engineering mass-deposition rate estimates, since the rms errors for predicting $\mathscr{R}$ over this entire range are found to be less than about 5 pct. in the important k_p/k_g, range below 10,000. A second type of plot was also used to test the accuracy of this correlation formula, viz: a normalized linear plot of exact vs correlation-values of $\log(\mathscr{R}/\mathscr{R}_c)/[\log(1/\mathscr{R}_c)]$. One such plot (Fig. 5)

[††] Equivalently, the additional parameter could have been chosen to be $\bar{v}/v_1 = \bar{N}$, the *mean* number of spherules in suspended aggregates of volume $\bar{v}$.

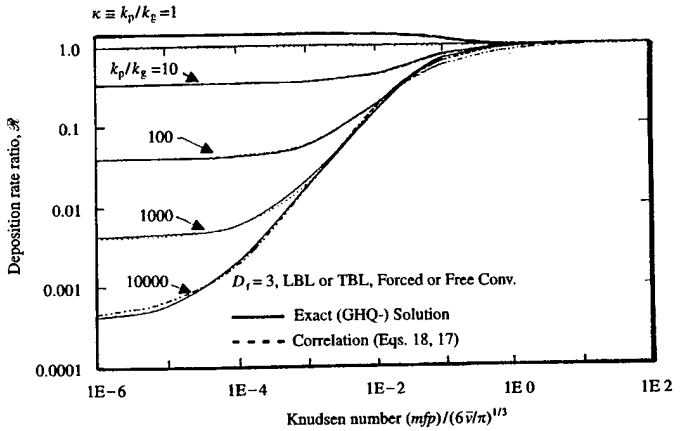

Fig. 4. Results for the deposition rate ratio $\mathscr{R}$ as a function of Knudsen number (based on mean particle size) and intrinsic thermal conductivity ratio $\kappa = k_p/k_g$ for dense spheres ($D_f = 3$), showing both GHQ-results (numerical quadrature) and the correlation formula (Eqs. (17) and (18)) developed in Section 3.7.

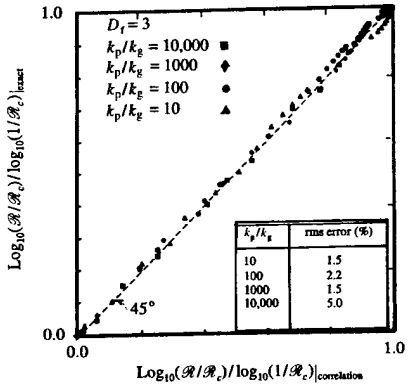

Fig. 5. Test of success of a simple correlation formula (Eqs. (18) and (17)) for $\mathscr{R}(\mathrm{Kn}, \kappa; D_f = 3)$ (Section 3.7).

exhibits only modest deviations from the 45° straight line corresponding to perfect agreement, and shows the success of equation (16) in tracking the inflection point locations (the point $\frac{1}{2}, \frac{1}{2}$ on these coordinates) for all values of k_p/k_g. Of course, if much greater accuracy is required, the numerical calculation of $\mathscr{R}$ for any desired combination of $Kn_{\bar{v}}$ and k_p/k_g would be quite efficient/straightforward using the above mentioned Gauss–Hermite quadrature procedure.

4.3. *Provisional* $\mathscr{R}\{Kn_{\bar{v}}, k_p/k_g\}$*-results for* $D_f = 1.7$

To illustrate the likely consequences of dealing with thermophoretically dominated deposition from a coagulation-aged population of *aggregated* particles, we have prepared Fig. 6, covering the same range of Knudsen numbers, $Kn_{\bar{v}}$, and intrinsic thermal conductivity ratios k_p/k_g, but for the particular case of $Kn_1 = 0.3$ (roughly corresponding to organic soot in a combustor at near 50 atm pressure). What is most noteworthy about these

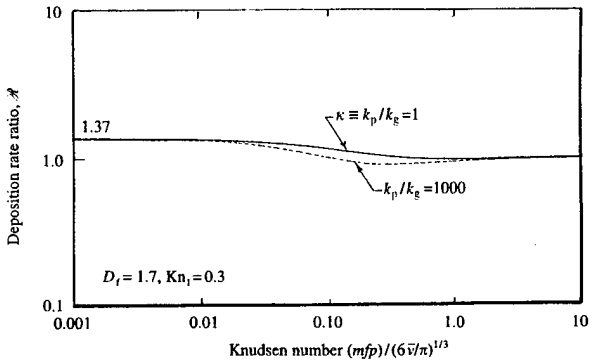

Fig. 6. Provisional results for the *deposition rate ratio* $\mathscr{R}$ as a function of Knudsen number (based on the mobility diameter of the mean aggregate size) and intrinsic (spherule) thermal conductivity ratio $\kappa = k_p/k_g$ for a coagulation-aged population of unsintered fractal aggregates with $D_f = 1.7$; $Kn_1 = 0.3$.

aggregate results is the rather modest departures from $\mathscr{R} = 1$ even at very high intrinsic thermal conductivity ratios (e.g. near 1000) and low Knudsen numbers based on mean aggregate size (i.e. in the near-continuum regime). Moreover, since the relevant *effective* thermal conductivity ratios often fall in the range: $1 < k_p/k_g < 2.12$, this approach leads to α- and $\mathscr{R}$-values *exceeding* unity. These (and similar) preliminary results provide the basis of the instructive numerical example discussed in Section 5.2.1 below, dealing with anticipated soot deposition rates from very high pressure combustors.

5. PROCEDURE FOR PRACTICAL USE

5.1. *Steps*

Thermophoretically dominated total mass deposition rates from flowing polydispersed aerosol populations can now be be conveniently calculated by sequentially following these tractable steps:

S1. First calculate "reference mass deposition rate" which would prevail due to thermophoresis in the same flow environment if all suspended particles had the mean size: $\bar{v} = \phi/N_p$, but using the size-independent Waldmann free-molecule limit value $((\alpha_T D)_p = 0.53852\ \nu_{gas})$ for the particle thermophoretic diffusivity (see, e.g., Rosner, 1980; Garcia-Ybarra and Rosner, 1989; Garcia-Ybarra and Castillo, 1997)

S2. Correct this "reference rate" by the dimensionless factor $\mathscr{R}$ calculated /correlated here "once- and-for-all" (Fig. 4, equations (18) and (17), Fig. 6) over the entire parameter range of practical interest (with Kn based on the length scale $(6\bar{v}/\pi)^{1/3}$)

This "two-step" strategy leads us to rational, efficient correlation formulae for $\mathscr{R}$ in all cases treated here; i.e. for all combinations of Knudsen number (based on mean size), thermal conductivity ratio, and for both extreme suspended particle morphologies ($D_f = 3$ or 1.7). Remarkably, *these results apply to either laminar or turbulent boundary layer situations, and for either "forced"- or "natural"-convection systems.*

Some important applications are briefly illustrated below.

5.2. *Illustrative numerical calculations and implications*

5.2.1. *Soot deposition rates from high-pressure combustors.* A technologically important application of our present methods is the prediction of soot deposition rates from very high-pressure hydrocarbon fuel/air combustors. As reported earlier, all published

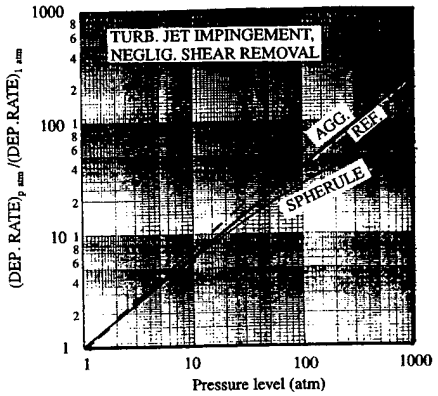

Fig. 7. Predicted *soot deposition rates* (normalized by that at 1 atm) in the absence of shear removal as a function of *pressure level* showing three limiting cases: (a) formally extrapolated to high pressure leaving the thermophoretic coefficient at the free-molecule level; (b) estimating actual aggregate thermophoretic diffusivities at the prevailing Knudsen numbers; and (c) deposition rates *if* soot spherules were *non-agglomerated* and 'monodispersed'; (All projections based on $\kappa = 1000$, constant soot mass loading, const. average aggregate size, and const. spherule size).

laboratory studies of soot *deposition* were carried out with laminar boundary layers at 1 atm., and few studies of soot *production* itself have been carried out much above atmospheric pressure. However, based on the available work of Miller (1978) (up to 50 atm) and Flower and Bowman (1986) (up to 20 atm), we will assume for purposes of illustration[88] that the diffusion flame soot *mass* fraction remains constant at a value near 0.5 pct (corresponding to soot *volume* fractions which increase linearly with pressure from ca. 0.8 ppm). Because high-pressure soot *morphology* studies donot appear to be available, we will provisionally assume that pressure level doesnot appreciably change the soot spherule diameter (near 30 nm) or the average number of spherules per aggregate (near 300). Now suppose that soot deposition rates could be measured downstream of a combustor like that operated at 1 atm. by Makel and Kennedy, 1991, and consider the deposition rates that would be expected at pressures up to, say, 1000 atm. for *turbulent* boundary layer flows of soot-laden combustion products past a cooled solid surface. Also suppose that this surface is maintained at $T_w/T_{jet} = 0.8$ and configured such that the wall shear rate at 1 atm is kept below ca. $8\,s^{-1}$ (to rule out soot re-entrainment ("rip-off") even at 1000 atm). In the calculations below all deposition rates will be expressed in multiples of the actual deposition rate at 1 atm., and the intrinsic carbon spherule thermal conductivity will be taken as ca. 1000 times that of the background gas (based on the thermal conductivity of pyrolytic graphite in the direction ("AB")- of the graphite sheets).

In the language of Sections 3.3 and 5.1, we first calculate the "reference" rates that would be expected in the same environment if all aggregates had the *free-molecule* thermophoretic diffusivity, 0.5385ν. In Fig. 7 this is plotted as a straight line of slope 0.8 (on equal cycle size log–log paper), corresponding to a reference deposition rate which increase as the 0.8 power of the pressure level. Moreover, at 1 atm the reference rate would be indistinguishable from the observed rate because $Kn_{\bar{v}}$ is about 0.67 and $Kn_1 \approx 11.4$ (cf. Fig. 6). In accord with the present formulation (Step 2, Section 5.1) actual aggregated soot deposition rates will be estimated by multiplying the reference rate (above) by the function $\mathscr{R}\{Kn_{\bar{v}}, k_p/k_g, D_f, Kn_1\}$ (again, see Fig. 6) evaluated at $D_f = 1.7$, $k_p/k_g = 1000$, for the prevailing values of the arguments $Kn_{\bar{v}}$ and Kn_1 (these shrink, repectively, to 0.67×10^{-3} and 0.0114 at 1000 atm).

[88] If the soot mass fraction, spherule size, and mean number of spherules per aggregate were subsequently found to have a non-negligible pressure dependence, this information could easily be incorporated.

The resulting predicted deposition rates are shown in Fig. 7 as the dashed curve marked: AGG ("predicted *aggregate* deposition rate"). Finally, it is interesting to consider the hypothetical soot deposition rate if aggregation were somehow prevented, or if the aggregates were somehow broken up prior to the deposition process. This curve, marked: "spherule deposition rate", is calculated by simply multiplying the reference rate by the term α/α_{fm} evaluated at $D_f = 3$, $k_p/k_g = 1000$, for the prevailing values of Kn_1 (Fig. 2). It is remarkable that at 1000 atmospheres the *spherule* deposition rate would be only about $\frac{1}{4}$ the reference rate, whereas the predicted *aggregate* rate would be fully ca. 137 pct of the reference rate, which is 251 times that achieved at 1 atm. Thus, while our aggregate thermophoretic diffusivity estimates are provisional, our two principal *conclusions*, expected to be "robust", are that:

C1: Actual large soot *aggregate* (say, $N > 30$) deposition rates at very high pressures will be perceptibly (but not appreciably) different from the rates formally expected using the *free-molecule* isolated sphere thermophoretic diffusivity.

C2: If aggregates could be prevented from forming, or broken up prior to thermophoretic deposition, then, apart from considerations of shear-induced removal, appreciable soot deposition rate *reductions* could be realized at very high pressures.

Apart from the fact that the reference deposition rate "line" for *laminar* boundary layer transport would have a slope of 0.5 rather than 0.8 (Fig. 7) these conclusions would carry over to fully LBL cases (if transition to turbulence didnot occur at 1000 atm due, say, to small dimensions). Incidentally, an interesting experimental corollary of our present findings is that, in contrast to the fortunate situation at 1 atm.(Rosner *et al.*, 1991; Dobbins and Megaridis, 1987), *thermophoretic sampling of intrinsically conductive materials (including carbon) at very high pressures would be "biased" (against small aggregates and isolated spherules)*, again, apart from considerations of shear-induced removal.

5.2.2. *Applications to interpretation/design of laboratory experiments involving the thermophoretic deposition of particle populations.* An interesting class of applications of the present formulation/results is in the design/interpretation of laboratory experiments involving thermophoretic deposition from particle populations. In our own group such experiments have been of two types, considered sequentially below. In the first category are experimental methods to study local soot concentration and morphology in atmospheric pressure flames by exploiting the laws of soot thermophoresis (Eisner and Rosner, 1986; McEnally *et al.*, 1997; Koylu *et al.*, 1997). In implementing these ideas it was assumed that even though the soot is comprised of aggregated spherules the free-molecule limit-laws were valid even though some aggregates in the suspension inevitably had overall dimensions comparable to or larger than the prevailing mean-free-path. Whether this produces any appreciable error in, say, the inferred soot volume fraction can now be easily estimated based on our present results—we need only compare the calculated $\mathscr{R}$-value (at the prevailing mean $Kn_{\bar{v}}$, k_p/k_g, D_f, Kn_1) with *unity* (the *fm*-value of $\mathscr{R}$). In the above mentioned experiments we can estimate typical values of these parameters as: $Kn_{\bar{v}} = 2.6$, $k_p/k_g = 800$ (upper limit at the prevailing gas temperature), $D_f = 1.7$, and $Kn_1 = 20$. Under these conditions one immediately sees from Fig. 6 (and even Fig. 4) that R is indeed near unity under the conditions studied by these authors. In the second category are experimental methods to study the laws governing thermophoretic particle deposition—a recent example being that of Konstandopoulos and Rosner, 1995, who worked with a narrow distribution of spray-pyrolysis-formed MgO particles centered about a diameter of 0.84 μm. In this case we estimate $Kn_{\bar{v}} = 0.5$, $k_p/k_g = 30$ (upper limit) and (based on TEM-images) $D_f = 3$. Reference to Fig. 4 suggests that for these parameters a coagulation-aged population would deposit with ca. $\mathscr{R} = 0.9$—i.e. some 10% less than that expected using the free-molecule value of the thermophoretic coefficient: $\alpha_T D_p/\nu$. Interestingly enough, it was reported that about a 7% reduction gave best overall agreement with the measured particle deposition rates at T_w/T_e near 0.8. Considering the fact that Fig. 4 is constructed for a broader (fully

"coagulation-aged") spread near $\sigma_g = 2.1$ (Fig. 3) at this $Kn_{\bar{v}}$ rather than that reported $(1.2)^3 = 1.7$), this agreement with our *a posteriori* "expectation" is encouraging.

Somewhat less directly related are estimates of the thermophoretic coefficient of suspended particles based on the observed location of thermophoretically created "particle stagnation planes" in atmospheric pressure laminar counterflow diffusion flames (Gomez and Rosner, 1993). While these inferences are not made based on total mass deposition rates to an immersed *solid* surface, it can be concluded that the flame-generated titania particle experiments of Gomez and Rosner were indeed run under conditions of negligible departure from the free-molecule limit value, whereas those of Nishioka *et al.* (1991) (using elutriated titania particles of mean diameter near 1 μm) were not. Since their averaged Kn-values were near 0.5, this is probably one of the reasons the latter investigators inferred $\alpha_T D_p$-values nearly half of the *fm*-limit theoretical value for a spherule (cf., Gomez and Rosner, 1993).

In the highest-pressure laboratory studies of flame-generated soot (see, e.g. Flower and Bowman, 1986; Miller, 1978), Knudsen numbers based on average aggregate mobility diameter are as small as 0.1, corresponding to $Kn_1 = O(1)$-values. Under these conditions (cf. Fig. 6) despite the high intrinsic thermal conductivity ratio for this system, we would expect noticeable but not dramatic departures from fm-limit behavior for the *aggregate* thermophoretic diffusivity, and, hence, inferred volume fractions (McEnally, *et al.*, 1997; Koylu *et al.*, 1997) or predicted mass deposition rates. The latter conclusion will be of special interest for anticipating/controlling soot deposition in/downstream of high pressure aeropropulsion combustors (Section 5.2.1). Ironically, our reasoning also leads us to expect (see also, Fig. 7) that, if aggregation of soot spherules could be prevented, or the aggregates could be broken up into sufficiently small "fragments", soot deposition rates at very high pressures but modest shear rates would be appreciably *reduced* (see Fig. 7, curve marked: spherule deposition, $D_f = 3$).

6. DISCUSSION OF ASSUMPTIONS; GENERALIZATIONS

It would be useful and prudent to at least outline the basis for our present idealizations (Assumptions 1–7, Section 2), and briefly present quantitative criteria for their validity in any new situation. In some cases due to space limitations, we can direct the reader to more detailed treatments that transcend these simplifications. The accuracy of our treatment of fractal aggregate thermophoresis (Sections 3.8 and 4.3) will have to remain for future research to determine—which accounts for our repeated use of the descriptor: *provisional* to describe our predictions for the case: $D_f = 1.7$.

"*Coagulation aged*" *aerosol populations?* The depositing population will be accurately described using this concept provided enough time has elapsed between particle inception (and any appreciable growth from the vapor) and arrival at the deposition location. If $\beta(v_g, v_g)$ is the coagulation coefficient for two particles of size v_g then this condition will be satisfied if the elapsed time is an adequate multiple of the *characteristic coagulation time*: $[\beta\{v_g, v_g\} \cdot N_p]^{-1}$. This required multiple is dependent on the spread of the post-nucleation aerosol and the prevailing Knudsen number (see, e.g. Vemury *et al.*, 1994) but is of the order of 12 for an initially "monodispersed" aerosol in the continuum limit. Coagulation-aged populations are known to be "single "mode" and nearly log-normal (only slightly negatively "skewed") and effective geometric mean spreads, σ_g, can be chosen to adequately retrieve the lower dimensionless moments needed for most deposition analyses[¶¶] (Rosner, 1989).

Definition of particle "state". The adequacy of particle *volume* and *fractal dimension* to define the size and morphology of a particle in the depositing population depends on the

[¶¶] It is noteworthy that our present deposition rate results (Figs 4 and 6) for arbitrary Kn_g cannot be compactly expressed in terms of appropriate fractional *moments* of the log-normal PSD (cf. Rosner, 1989, 1998; Rosner and Tassopoulos, 1989). However, in the near-*fm* limit, note the presence of $\mu_{4/3}$ and $\mu_{5/3}$ in the truncated expression equation (14).

possible deposition rate importance of other uncorrelated morphological variables, such as *particle surface area* (see, e.g. Koch and Friedlander, 1990; Tandon and Rosner, 1998). We may consider the present analysis adequate in the two well-understood limiting cases of rapid- or slow-coalescence rates. This can be quantified in terms of the *ratio* of the above mentioned characteristic *coagulation time*, and the characteristic time associated with surface-energy-driven spherule *coalescence* in the prevailing environment (Tandon and Rosner, 1998), which can either be very large (leading to $D_f = 3$) or very small (leading to $D_f = 1.7$).

Thermophoretic domination. In earlier work we have shown that particle transport by thermophoresis will dominate Brownian diffusion whenever the dimensionless parameter B_T defined below is large compared to unity (see, e.g. Rosner *et al.*, 1992).

$$B_T = (\alpha_T D_p/\nu)\cdot(\Delta T/T_w)\cdot(\mathrm{Pr})^{1/3}(\mathrm{Sc})^{2/3}. \tag{19}$$

But, since the "property" factors $\alpha_T D_p/\nu$ and Pr are each of order unity, and, for aerosol systems $\mathrm{Sc} \gg 1$, the temperature contrast parameter, $\Delta T/T_w$, would have to be exceedingly small for convective-diffusion to play a non-negligible role in determining particle deposition rates, especially if the suspended particles were near the free-molecule extreme or relatively non-conducting. For much larger particles in turbulent thermal boundary layers we must consider the onset of "eddy impaction" effects which could ultimately become important enough to "compete" with thermophoresis. This is a particle inertia-sensitive process which would only become important when the particle stopping time, t_p, exceeds the product $(\frac{1}{2})B_T\cdot(\delta_{m,o}/u_*)$, where $\delta_{m,o} = L/\mathrm{Nu}_{m,o}$ is the mass transfer BL thickness in the absence of thermophoresis or particle inertia, and $u_* = U(C_f/2)^{1/2}$ is the so-called "friction velocity" (see, e.g. Rosner and Fernandez de la Mora, 1982; Rosner, 1986; Rosner and Tassopoulos, 1989). On inspection of the above mentioned criteria, it is interesting to observe that the the domain of applicability of our present deposition rate treatment is even broader for the fractal aggregate case (slow coalescence), than for the dense spherical particle (rapid-coalescence) case. Also, since the particle sedimentation speed can be written: gt_p, thermophoresis will dominate gravitational sedimentation whenever t_p is much smaller than the product: $(\alpha_T D_p/\nu)\cdot(\Delta T/T_w)\cdot[\nu/(g\delta_h)]$, where δ_h is the prevailing *thermal* BL thickness, $L/\mathrm{Nu}_{h,o}$, at the deposition location.

Dependence of mass transfer coefficient on $\alpha = \alpha_T D_p/\nu$. The condition $B_T \gg 1$ above is necessary but not sufficient for the mass transfer coefficient to depend nearly *linearly* on $\alpha \equiv \alpha_T D_p/\nu$. From the viewpoint of Gokoglu and Rosner (1984) it is also necessary that particle mass fraction reduction across the thermal BL (outside the thin Brownian diffusion sublayer) be negligible, which leads to the additional condition: $(\alpha_T D_p/\nu)\cdot(\mathrm{Pr})\cdot(\Delta T/T_w) \ll 1$. This additional condition will normally be satisfied when the absolute temperature ratio T_w/T_e does not fall much below about 0.8. When wall cooling is much more severe there would be an associated *reduction* in the sensitivity of the mass transfer coefficient to $\alpha \equiv \alpha_T D_p/\nu$, which should be taken into account in our quadratures, especially for the smallest particles in the population. However, this observation also suggests that our conclusions about the insensitivity of total *aggregate* mass deposition rate to the population-averaged Knudsen number, irrespective of k_p/k_g (Section 4.3 and Fig. 6) will be even more accurate for highly cooled walls!

Uniformity of intrinsic particle thermal conductivity and density. It seems likely that if the aerosol population is "coagulation-aged" (in the sense above) at the site of deposition, it will also be nearly physically "well mixed". This implies that the prevailing particle thermal conductivity and mass density at the deposition site will be nearly that expected by physically "blending"–coalescing the initial populations. More quantitative validity criteria will be possible based on multi-variate aerosol coagulation research in progress (e.g. Tandon and Rosner, 1998), but single chemical substance aerosol are ubiquitous and justify our present emphasis on this situation, especially in view of our stated objectives.

Neglect of high particle-mass-loading effects. This situation has been dealt with in our earlier research on the industrially significant deposition process of optical wave-guide manufacture (see, e.g. Rosner and Park, 1988; Rosner, 1997). Particle volume fractions in many environmentally significant aerosol applications are small enough (often below 0.1 ppm) to allow these complications to be safely neglected.

Neglect of BL coagulation effects: Low particle volume fractions are also consistent with the neglect of particle-particle interactions within the mass transport BL. Moreover, except for the case of thermally conductive particles in the Knudsen transition regime, even if Brownian coagulation did occur within the thermal BL, it would not modify the operative thermophoretically dominated mass transfer coeffcient (Park and Rosner, 1988). In any case, a *sufficient* condition for the neglect of Brownian coagulation effects will be that the above mentioned coagulation time be long on the time scale:

$$(\alpha_T D_p/\nu)^{-1}\cdot(\Delta T/T_w)^{-1}\cdot(\mathrm{Pr})^{-1}\cdot(\delta_h^2/\alpha_h),$$

where α_h is the gas mixture *thermal* diffusivity.

Irreversible particle capture by the wall: Threshold velocities for particle/surface "rebound" (see, e.g. Konstandopoulos and Rosner, 1997; Rosner *et al.*, 1994; Rosner and Tandon, 1995) from a clean cold solid typically far exceed those associated with thermophoretic drift—i.e.: $(\alpha_T D_p/\nu)\cdot(\mathrm{Pr})\cdot(\Delta T/T_w)\cdot(\alpha_h/\delta_h)$. Accordingly, irreversible particle "trapping" by the cold solid surface is fully consistent with the abovementioned physical model, unless the shear stress at the gas/deposit interface is large enough to overcome the adhesive forces holding spherules to one another, and/or to the underlying target. In the 1 atm. ethylene/air soot deposition experiments of Makel and Kennedy (1991), this occurred at shear rates of the order of $2000\ \mathrm{s}^{-1}$.

We conclude from these considerations that the mathematical model investigated here (Section 2) has a broad domain of applicabilitiy even for aerosols comprised of dense spherical particles ($D_f = 3$). Ironically, we expect the domain of validity to be increased (without the need to specify many additional dimensionless parameters) for cases involving suspended *aggregates* (with $D_f = 1.7$), with the principal remaining uncertainty being the absolute accuracy of our evaluation of $\alpha_T D_p$ for such particles (Section 3.8).

7. CONCLUSIONS; CURRENT/FUTURE WORK

Previous papers from this group (Rosner, 1989, 1998; Rosner and Tassopoulos, 1989, 1991, 1992) have shown that total mass deposition rates from a stream containing coagulation-aged polydispersed aggregated particles can be predicted by systematically correcting (for polydispersity) results first calculated for the (hypothetical) case of *monodispersed particles* (with the same volume fraction, $\bar{v}N_p$) in the same environment. This "first step" result (Section 5.1) is then corrected for polydispersity by using the $\mathscr{R}$-factors calculated/displayed here (Fig. 4 (or correlation equations (17) and (18), Fig. 6) for the particular case of deposition by the non-power-law mechanism of *thermophoresis* (cf., isothermal convective-diffusion, gravitational sedimentation, or "eddy impaction" treated earlier (Rosner, 1989; Rosner and Tassopoulos, 1989; Rosner and Khalil, 1997) for *laminar or turbulent*, forced- or free-convective flow of suspended particles in the Knudsen transition regime. Using this convenient but rational formalism above, we have also estimated how suspended particle *morphology* (i.e. the presence of unsintered "fractal aggregates" with $D_f = 1.7$) would influence thermophoretically dominated mass transfer rates, concluding that, irrespective of intrinsic thermal conductivity, thermophoretically dominated deposition rates would be remarkably insensitive to Knudsen number (corresponding to surprisingly large *aggregate* deposition rates (e.g., carbonaceous soot) in the high pressure (continuum) limit. We illustrated in Section 5 the extent to which this strategy/set of results simplifies engineering calculations of mass deposition rates from polydispersed aerosol populations. We also note that the laws underlying our calculations (Section 3) have been rather well established based on both earlier theoretical analysis (see, e.g. Rosner and Fernandez de la Mora, 1982; Garcia-Ybarra and Castillo, 1997) and laboratory experimentation (Rosner and Kim, 1986; Makel and Kennedy, 1991; Gomez and Rosner, 1993; Konstandopoulos and Rosner, 1995). Thus, if the validity criteria discussed in Section 6 are indeed met, the results reported here can be used with considerable confidence

even in the absence of further "direct" validation. Ironically, the domain of validity is expected to be greater for suspended aggregates ($D_f = 1.7$) than for the more familiar case of spherical particles ($D_f = 3$), however our procedure for estimating fractal aggregate thermophoretic diffusivities (Section 3.8) must be regarded as provisional, and may require systematic corrections.

Deposition rates from aggregated particle populations (Sections 3.8 and 4.3) can change not only due to coagulation but also due to finite-rate *aggregate restructuring* processes—e.g. those brought about by surface-energy driven sintering at high temperatures (Xing *et al.*, 1997, 1999; Tandon and Rosner, 1996, 1999) or, say, aggregate-induced vapor capillary condensation. The implications of such finite-rate restructuring for particle deposition rates are currently being considered in the light of the formalism above and recent Monte-Carlo coagulation–coalescence simulations of spatially uniform particle populations distributed both with respect to particle *volume* and particle surface *area* (Tandon and Rosner, 1998). Merely comparing Figs 4 and 6, corresponding, respectively, to the limiting cases $D_f = 3$ and 1.7, reveals the maximum extent to which (a) sintering will *reduce* the rate of thermophoretic deposition from populations of conductive materials, and, perhaps more surprising, (b) *aggregation* is now expected to *increase* the rate of *thermophoretic* deposition in high pressure but low shear rate, non-isothermal systems (e.g. ordinary carbonaceous soot in/downstream of high-pressure combustors).

It is anticipated that these new deposition rate methods, results, correlations and conjectures will prove useful to simplify and enhance existing software (often large and complex codes containing arguable deposition-rate subroutines) developed in recent decades for specific industries.

Acknowledgements—It is a pleasure to acknowledge the financial support of AFOSR (Yale Grant: 97-1-0266), NASA (Grant: NAG 3-1951), AGARD/NATO (Grant P-125 with IST-Lisbon), and the Yale HTCRE Lab *Industrial Affiliate*: duPont. We also acknowledge helpful discussions with J. L. Castillo, M. Epstein, P. Garcia-Ybarra, S. A. Gokoglu, A. G. Konstandopoulos, R. McGraw, J. Fernandez de la Mora, T. Farias, A. V. Filippov, A. Brasil, M. Kumar, D. W. Mackowski, L. Talbot, P. Tandon, and Y. Xing.

29

REFERENCES

Abramowitz, M. and Stegun, I. A. (1964) *Handbook of Mathematical Functions.* National Bureau of Standards, Wash. DC, Appl. Maths. Series #55; Reprinted by Dover Press, NY.

Batchelor, G. and Shen, C. J. (1985) Thermophoretic deposition of particles in gas flowing over cold surfaces. *J. Colloid Int. Sci.* **107,** 21–37.

Dobbins, R. A. and Megaridis, C. M. (1987) Morphology of flame-generated soot as determined by thermophoretic sampling. *Langmuir (ACS)* **3,** 254–259.

Eisner, A. D. and Rosner, D. E. (1986) Experimental and theoretical studies of submicron particle thermophoresis in combustion gases. *PCH* (Physicochemical Hydrodynamics (Pergamon)) 7(2/3), 91–100.

Epstein, M., Hauser, G. M. and Henry, R. E. (1985) Thermophoretic deposition of particles from natural convectiuon flow from a vertical plate, *ASME J. Heat Transfer* **107,** 272–276.

Flower, W. L. and Bowman C. T. (1986) Soot production in axisymmetric laminar diffusion flames at pressures from one to ten atmospheres. 21*st Symp. (Int.) on Combustion.* Comb. Inst., Pittsburgh, PA, pp. 1115–1124.

Friedlander, S. K. (1977) *Smoke, Dust and Haze.* Wiley, New York.

Garcia-Ybarra, P. and Rosner, D. E. (1989) Thermophoretic properties of non-spherical particles and large molecules. *A.I.Ch.E. J.* **35**(1), 139–147.

Garcia-Ybarra, P. and Castillo, J. L. (1997) Mass transfer dominated by thermal diffusion in laminar boundary layers. *J. Fluid Mech.* **336,** 379–409

Gokoglu, S. A. and Rosner, D. E. (1984) Correlation of thermophoretically-modified small particle diffusional deposition rates in forced convection systems with variable properties, transpiration cooling and/or viscous dissipation. *Int. J. Heat Mass Transfer* **27**(5), 639–646; see, also, *AIAA J.* **24**(1), 172–179 (1986).

Gomez, A. and Rosner, D. E. (1993) Thermophoretic effects on particles in counterflow laminar diffusion flames. *Combust. Sci. Technol.* **89,** 335–362.

Goren, S. L. (1977) Thermophoresis of aerosol particles in the laminar boundary layer on a flat plate. *J. Colloid Int. Sci.* **61,** 277–285.

Helble, J. J. and Sarofim, A. F. (1989) Factors determining the primary particle size of flame-generated inorganic aerosols. *J. Colloid Int. Sci.* **128,** 419–427.

Koch, W. and Friedlander, S. K. (1990) The effect of particle coalescence on the surface area of a coagulating aerosol. *J. Colloid Int. Sci.* **140,** 419–427.

Konstandopoulos, A. G. and Rosner, D. E. (1995) Inertial effects on thermophoretic transport of small particles to walls with streamwise curvature, I. Theory. *Int J. Heat Mass Transfer* **38**(12), 2305–2315; II. Experiment, *Int J. Heat Mass Transfer* **38**(12), 2317–2327.

Konstandopoulos, A. G. and Rosner, D. E. (1997) The initial sticking fraction of inertially impacting partiucles on cylindrical and spherical collectors. *J. Aerosol Sci.* **28** (Suppl. #1), S89–S90.

Koylu, U. O., Xing, Y. and Rosner, D. E. (1995) Fractal morphology analysis of combustion-generated aggregates using angular light scattering and electron microscope images. *Langmuir* (ACS) **11**(12), 4848–4854.

Makel, D. B. and Kennedy, I. M. (1991) Experimental and numerical investigation of soot deposition in laminar stagnation point boundary layers. *Proc. 23d. Symp. (Int.) on Combustion,* The Combust. Inst., Pittsburgh PA, pp. 1551–1557.

Megaridis, C. M. and Dobbins, R. A. (1990) Morphological description of flame-generated materials. *Combust. Sci. Technol.* **71,** 95–109.

Neimark, A. V., Koylu, U. O. and Rosner, D. E. (1996) Extended characterization of combustion-generated aggregates: self-affinity and lacunarities. *J. Colloid Interface Sci.* **180,** 590–597.

Nishioka, M., Uchida, N. and Takeno, T. (1991) Thermophoretic behavior of submicron particles in diffusion flames. *Proc. 13th ICODERS Mtg.,* AIAA Publishers, Nagoya, Japan (1993).

Otto, E., Stratmann, F., Fissan, H., Vemury, S. and Pratsinis, S. E. (1994) Quasi-self-preserving log-normal size distributions in the transition regime. *Part./Part. Syst. Char.* (VCH) **11,** 359–366.

Park, H. M. and Rosner, D. E. (1989) Combined inertial and thermophoretic effects on particle deposition rates in highly loaded dusty gas systems. *Chem. Engng Sci.* **44**(10), 2233–2244.

Park, H. M. and Rosner, D. E. (1989) Boundary layer coagulation effects on the size-distribution of thermophoretically deposited particles. *Chem. Engng Sci.* **44**(10), 2225–2231.

Rosner, D. E. (1980) Thermal (Soret) diffusion effects on interfacial mass transport rates. *Physicochemical Hydrodynamics* (PCH), **1,** 159–185, Pergamon Press, Oxford.

Rosner, D. E. (1989) Total mass deposition rates from polydispersed aerosols. *A.I.Ch.E. J.* **35**(1), 164–167.

Rosner, D. E. (1997) Combustion synthesis and materials processing. *Chem. Engng Educ.* (ASEE) **34**(4), 228–235.

Rosner, D. E. (1998a) Soot morphology and high pressure effects on thermophoretically-dominated deposition rates, (in preparation); see also: 27*th Combust. Symp.* Poster W5G11-Boulder CO, August 1998.

Rosner, D. E. (1998b) Knudsen transition-effects on total mass deposition rates from 'coagulation-aged' aerosol populations. AIChE Particle Technology Forum; Proc. *Symp. on Advanced Technologies for Particle Production,* Nov. 15–20, 1998. Vol. **1,** pp. 357–362, Miami Beach, Florida.

Rosner, D. E. and Fernandez de la Mora, J. (1982) Small particle transport across turbulent non-isothermal boundary layers. *ASME J Engng Power* **104,** 885–894.

Rosner, D. E. and Kim, S. S. (1984) Optical experiments on thermophoretically augmented submicron particle deposition from Dusty high temperature gas flows. *The Chem. Engng J.* (Elsevier) **29**(3), 147–157.

Rosner, D. E. and Tassopoulos, M. (1989) Deposition rates from polydispersed particle populations of arbitrary spread, *A.I.Ch.E. J.* **35**(9), 1497–1508. [As indicated in the captions, in the ascissae of Figs. 5, 6, 10, 11 the volume shown in the numerator should have an overbar, to indicate the *mean* particle volume in the population.]

Rosner, D. E. and Tassopoulos, M. (1991) Direct solutions to the canonical 'Inverse' problem of aerosol sampling theory: coagulation and size-dependent wall loss corrections for log-normally distributed aerosols in upstream sampling tubes. *J. Aerosol Sci.* **22**(7), 843–867.

Rosner, D. E., Garcia-Ybarra, P. and Mackowski, D. W. (1991) size and structure-insensitivity of the thermophoretic transport of aggregated soot particles in gases. *Combust. Sci. Technol.* **80,** 87–101.

Rosner, D. E. and Khalil, Y. F. (1997) Morphology effects on polydispersed aerosol deposition rates. *Trans. Amer. Nucl. Soc.* **77** TANSAO 77-1-560, 425–427.

Rosner, D. E., Mackowski, D. W, Tassopoulos, M., Castillo, J. L. and Garcia-Ybarra, P. (1992) Effects of heat transfer on the dynamics and transport of small particles in gases. *I&EC-Res.* (*ACS*) **31**(3), 760–769.

Rosner, D. E. and Park, H. M. (1988) Thermophoretically augmented mass, momentum and energy transfer rates in high particle mass-loaded laminar forced convection systems. *Chem. Engng Sci.* **43**(10), 2689–2704. (In the expressions for t(coag) (Eqs. A5-1, A5-3) restore the exponent -1 which was left out in typesetting).

Rosner, D. E. (1990) *Transport Processes in Chemically Reacting Flow Systems.* Butterworth-Heinemann, (Stoneham MA), 3d Printing sold out; for 4th printing contact author directly; 2d ed. in preparation.

Rosner, D. E., Tandon, P., Konstandopoulos, A. G. and Tassopoulos, M. (1994) Prediction/correlation of particle deposition rates from dilute polydispersed flowing suspensions and the nature/properties of resulting deposits. *Proc. 1st Int. Particle Technology Forum* (AIChE, IChE), Denver CO, August 1994; Paper 68h, Vol. II, pp. 374–381.

Rosner, D. E. and Tandon, P. (1994) Prediction and correlation of accessible area of large multi-particle aggregates. *A.I.Ch.E. J.* **40**(7), 1167–1182.

Rosner, D. E. and Tandon, P. (1995) Rational prediction of inertially induced particle deposition rates for a cylindrical target in a dust-laden stream. *Chem. Engng Sci.* **50**(21), 3409–3431.

Talbot, L. (1980) Thermophoresis—a review. *Proc. 12th Int. Symp. on Rarefied Gasdynamics,* AIAA Publishers, Wash. DC, pp. 467–488.

Tandon, P. and Rosner, D. E. (1995) Translational Brownian diffusion coefficient of large (multi-particle) suspended aggregates. *Ind Eng Chem-Res.* (ACS) **34,** 3265–3277. [Our pseudo-homogeneous mathematical model/finite-analytical computational technique has also been used, seemingly independently, by S. Veerapaneni and M. R. Weisner, *J. Colloid Int. Sci.* **177,** 45 (1996).]

Tandon, P. and Rosner, D. E. (1999) Monte-Carlo simulation of particle aggregation and restructuring. *J. Colloid Interface Sci.* **213,** 273–286.

Tandon, P. and Rosner, D. E. (1996) Sintering kinetics and transport property evolution of large multi-particle aggregates. *Chem. Engng Commun.* **151,** 147–158.

Vemury, S., Kusters, K. A. and Pratsinis, S. E. (1994) Time-lag for attainment of the self-preserving size distribution by coagulation. *J. Colloid Interface Sci.* **165,** 53–59.

Vemury, S., and Pratsinis S. E. (1995) Self-preserving size distributions of agglomerates. *J. Aerosol Sci.* **175**(2), 175–185.

Williams, M. M. R. and Loyalka, S. K. (1991) *Aerosol Science and Theory*. Pergamon Press, New York.
Wu, M. K. and Friedlander, S. K. (1993) Enhanced power-law agglomerate growth in the free-molecule regime. *J. Aerosol Sci.* **24**(3), 273–282.
Xing, Y., Koylu, U. O. and Rosner, D. E. (1996) Synthesis and restructuring of inorganic nano-particles in counterflow diffusion flames. *Combust. and Flame* **107**, 85–102.
Xing, Y., Koylu, U. O., Tandon P. and Rosner, D. E. (1997) Morphological evolution of oxide nano-particles in laminar counterflow diffusion flames—measurements/modelling. *A.I.Ch.E. J.* **43**(11A), 2641–2649.
Xing, Y. and Rosner, D. E. (1999) Prediction of spherule size in gas phase nano-particle synthesis. Invited Paper for *J. NanoParticle Res.* (Kluwer); Special Issue on *Gas Phase Synthesis of Nano-Particles* (Summer 1999).
Xing, Y., Koylu, U. O. and Rosner, D. E. (1999) *In situ* light scattering measurements of morphologically evolving flame-synthesized oxide nano-aggregates. *J. Appl. Opt.* **38**(12), 2686–2697 (April 20).

30